

Spring 2016

Tunable controlled release of molecular species from Halloysite nanotubes

Divya Narayan Elumalai
Louisiana Tech University

Follow this and additional works at: <https://digitalcommons.latech.edu/dissertations>

 Part of the [Atomic, Molecular and Optical Physics Commons](#), and the [Nanoscience and Nanotechnology Commons](#)

Recommended Citation

Elumalai, Divya Narayan, "" (2016). *Dissertation*. 124.
<https://digitalcommons.latech.edu/dissertations/124>

This Dissertation is brought to you for free and open access by the Graduate School at Louisiana Tech Digital Commons. It has been accepted for inclusion in Doctoral Dissertations by an authorized administrator of Louisiana Tech Digital Commons. For more information, please contact digitalcommons@latech.edu.

**TUNABLE CONTROLLED RELEASE OF MOLECULAR
SPECIES FROM HALLOYSITE NANOTUBES**

by

Divya Narayan Elumalai, M.S., M.S.

**A Dissertation Presented in Partial Fulfillment
of the Requirements for the Degree of
Doctor of Philosophy**

**COLLEGE OF ENGINEERING AND SCIENCES
LOUISIANA TECH UNIVERSITY**

May 2016

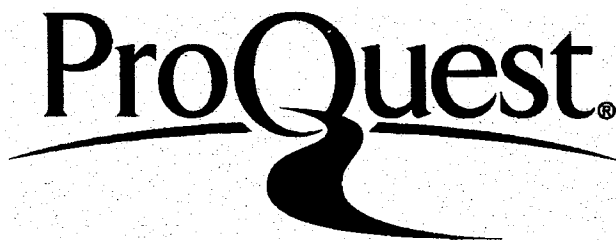
ProQuest Number: 10300727

All rights reserved

INFORMATION TO ALL USERS

The quality of this reproduction is dependent upon the quality of the copy submitted.

In the unlikely event that the author did not send a complete manuscript and there are missing pages, these will be noted. Also, if material had to be removed, a note will indicate the deletion.



ProQuest 10300727

Published by ProQuest LLC(2017). Copyright of the Dissertation is held by the Author.

All rights reserved.

This work is protected against unauthorized copying under Title 17, United States Code.
Microform Edition © ProQuest LLC.

ProQuest LLC
789 East Eisenhower Parkway
P.O. Box 1346
Ann Arbor, MI 48106-1346

LOUISIANA TECH UNIVERSITY

THE GRADUATE SCHOOL

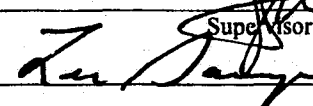
November 09 2015

Date

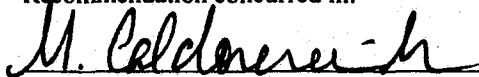
We hereby recommend that the dissertation prepared under our supervision
by Divya Narayan Elumalai, M.S.,M.S.

entitled Tunable Controlled Release of Molecular Species from Halloysite Nanotubes

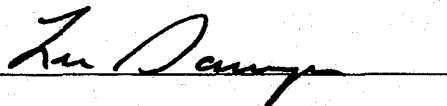
be accepted in partial fulfillment of the requirements for the Degree of
Doctor of Philosophy in Engineering Physics


Supervisor of Dissertation Research

Head of Department
Department of Physics and Chemistry
Department

Recommendation concurred in:



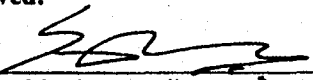
Yuri Lvov



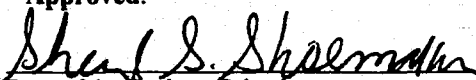
Zeno D. Guzman

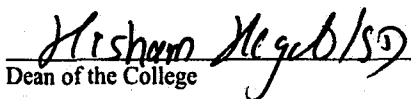
Advisory Committee

Approved:


Director of Graduate Studies

Approved:


Dean of the Graduate School


Dean of the College

ABSTRACT

Encouraged by potential applications in rust coatings, self-healing composites, selective delivery of drugs, and catalysis, the transport of molecular species through Halloysite nanotubes (HNTs), specifically the storage and controlled release of these molecules, has attracted strong interest in recent years. HNTs are a naturally occurring biocompatible nanomaterial that are abundantly and readily available. They are aluminosilicate based tubular clay nanotubes with an inner lumen of 15 nm and a length of 600-900 nm. The size of the inner lumen of HNTs may be adjusted by etching. The lumen can be loaded with functional agents like antioxidants, anticorrosion agents, flame-retardant agents, drugs, or proteins, allowing for a sustained release of these agents for hours. The release times can be further tuned for days and months by the addition of tube end-stoppers. In this work a three-dimensional, time-quantified Monte Carlo model that efficiently describes diffusion through and from nanotubes is implemented. Controlled delivery from Halloysite Nanotubes (HNT) is modeled based on interactions between the HNT's inner wall and the nanoparticles (NP) and among NPs themselves. The model was validated using experimental data published in the literature. The validated model is then used to study the effect of multiple parameters like HNT diameter and length, particle charge, ambient temperature and the creation of smart caps at the tube ends on the release of encapsulated NPs. The results show that release profiles depend on the size distribution of the HNT batch used for the experiment, as delivery is sensitive to HNT

lumen and length. The effect of the addition of end-caps to the HNTs, on the rate of release of encapsulated NPs is also studied here. The results show that the release profiles are significantly affected by the addition of end caps to the HNTs and is sensitive to the end-cap pore lumen. A very good agreement with the experiment is observed when a weight averaged release profile is compared to the experimental profile. Although the NP dynamics is temperature dependent, the effect is minimum within the range of temperatures relevant to biomedical applications, but will be relevant for other applications at temperatures significantly different from room temperature. This model can be used to predict the best conditions for a particular delivery need. One of the possible outcomes of this work is the development of more complex models for HNT-NP interaction various materials used in bioanalytical devices. These models will then be introduced into continuum models of transport in such devices. This work will leverage interaction potential development efforts under the LA-SiGMA grant, to enable multi-scale simulations involving interactions between biomaterials for which such potentials are unknown.

APPROVAL FOR SCHOLARLY DISSEMINATION

The author grants to the Prescott Memorial Library of Louisiana Tech University the right to reproduce, by appropriate methods, upon request, any or all portions of this Dissertation. It is understood that "proper request" consists of the agreement, on the part of the requesting party, that said reproduction is for his personal use and that subsequent reproduction will not occur without written approval of the author of this Dissertation. Further, any portions of the Dissertation used in books, papers, and other works must be appropriately referenced to this Dissertation.

Finally, the author of this Dissertation reserves the right to publish freely, in the literature, at any time, any or all portions of this Dissertation.

Author *Jayaraman Elumalai*

Date 05/05/2016

DEDICATION

To God, the source of everything I know and everything that I have yet to learn.

To my parents, Mr. Munuswamy Elumalai and Mrs. Rama Elumalai, and my sister, Anusha Elumalai, for their unwavering encouragement, support and guidance without which I couldn't have completed this project.

TABLE OF CONTENTS

ABSTRACT.....	iii
DEDICATION.....	vi
LIST OF TABLES.....	ix
LIST OF FIGURES.....	x
ACKNOWLEDGEMENTS.....	xiii
CHAPTER 1 INTRODUCTION AND LITERATURE REVIEW.....	1
1.1 Background.....	1
1.2 Nanotubes.....	2
1.3 Controlled Release.....	4
1.4 Diffusion.....	5
1.5 Halloysite Nanotubes.....	11
1.6 Motivation.....	14
1.7 HNTs with Endcaps.....	16
CHAPTER 2 MATERIALS AND METHODS.....	20
2.1 Model and Simulation Method.....	20
2.2 NP-Wall Interaction.....	22
2.3 NP-NP Interaction.....	26
2.4 Introducing Time in the Algorithm.....	27
2.5 Modelling Pores/Endcaps at Tube Ends.....	29
2.6 NP-Pore Wall Interaction.....	31
2.7 Experimental Conditions Nanotube Loading/Release.....	34

CHAPTER 3 RESULTS AND DISCUSSION	35
3.1 Validation of the Model	35
3.2 Effect of HNT Lumen	44
3.3 Effect of NP Charge	46
3.4 HNT Lumen Corrected Release Profiles	48
3.5 Effect of HNT Length	49
3.6 HNT Lumen and Length Corrected Release Profiles	50
CHAPTER 4 SUSTAINED RELEASE FROM HNTs WITH ENDCAPS	52
4.1 HNTs with Spherical Endcaps	52
4.2 HNTs with Planar Endcaps	55
4.3 Charged Endcaps	57
CHAPTER 5 DELIVERY DUE TO EXTERNAL STIMULI	59
5.1 Effect of HNT Length	59
5.2 Three Phase Release	62
5.3 Effect of Ambient Temperature	63
5.4 Effect of Surface Potential And pH	66
CHAPTER 6 CONCLUSIONS	70
CHAPTER 7 FUTURE WORK	73
APPENDIX A: FLOW CHART OF THE ALGORITHM	75
BIBLIOGRAPHY	77

LIST OF TABLES

Table 2.1: Physical properties of the four different NPs used in this work	33
Table 3.1: Comparison of release times from micro-crystals and HNTs.....	38
Table 3.2: Interpretation of diffusional release mechanisms from cylindrical channels .	41
Table 3.3: Parameters from fitting different models to the release profiles from HNTs.	43
Table 5.1: Mean square deviation from the experimental prediction of the release profile for dexamethasone. For the first three cases, all HNTs are of a 1µm in length.....	61

LIST OF FIGURES

Figure 2.1: a) TEM and b)SEM images of a clay nanotube batch, c) Schematic cross section of a charged cylindrical nanotube with ions inside used as a model for this work	21
Figure 2.2: Geometry considered as a model for this work.....	25
Figure 2.3: a) Single opening pore b) Perforated pore	30
Figure 3.1: Simulation results compared to experimentally available release profiles for a) 2-Acetoxy benzoic Acid b) dexamethasone, c) furosemide and d) nifedipine, from a 12 nm lumen HNT	36
Figure 3.2: Simulation results compared to experimentally available release profiles for a) 2-Acetoxy benzoic Acid, b) dexamethasone, c) furosemide and d) nifedipine d), from a 12 nm lumen HNT	37
Figure 3.3: Experimentally determined HNT inner lumen diameter distribution	38
Figure 3.4: Diffusion models compared to simulated release profiles for a) 2-Acetoxy benzoic Acid b) dexamethasone, c) furosemide, d) nifedipine.....	43
Figure 3.5: a) Simulated release profiles of dexamethasone molecules from HNTs of different radii. b) Time needed for a given percentage of particles to be releases vs lumen diameter.....	44
Figure 3.6: Weighted average release profiles of dexamethasone molecules from HNTs of different radii, for various inner lumen diameter distributions.....	46
Figure 3.7: a) Release profiles for repulsive interactions between the wall and the particles for different radii. b) Release profiles for attractive interactions between the wall and the particles for different radii.....	47
Figure 3.8: a) Release profiles of dexamethasone-like particles with different charges from HNTs of lumen 15nm. b) Time needed for 20%, 50% and 90% release of NPs Vs NP charge	48
Figure 3.9: Comparing the experimental and weighted average simulated release profiles of a) 2-acetoxy benzoic acid. b) dexamethasone, c) furosemide and d) nifedipine	49

Figure 3.10: a) Simulated release profiles of dexamethasone molecules as a function of tube length b) Length distribution of a sample of HNT	50
Figure 3.11: Comparing the experimental and weighted average simulated release profiles of a) 2-acetoxy benzoic acid.[134] b) dexamethasone, c) furosemide and d) nifedipine	51
Figure 4.1: Schematic depicting typical end cap formation.	52
Figure 4.2: Release profiles of dexamethasone Molecules from HNTs with spherical endcaps for different pore radii.	53
Figure 4.3: Release profiles of dexamethasone Molecules from HNTs with charged spherical endcaps for different pore radii.....	54
Figure 4.4: Release profiles of dexamethasone Molecules from HNTs with spherical endcaps and flat endcaps with pore of diameter 3nm.....	55
Figure 4.5: a) Release profiles of dexamethasone molecules from HNTs with perforated endcaps for different values of A by changing the number of pores by keeping the radius to 1nm b) Release profiles of dexamethasone molecules from HNTs with perforated endcaps with fixed number of pores (2) but different radii.....	56
Figure 4.6: Simulated release profiles of dexamethasone NPs for two distinct configurations of planar endcaps	57
Figure 4.7: Release profiles of dexamethasone from 2 different perforated pore openings for both charged and uncharged pores	58
Figure 5.1: a) TEM images of HNTs showing diversity in HNTs Lumen distribution. b) SEM images showing the diversity in HNT size	60
Figure 5.2: a) Simulated release profiles of dexamethasone molecules as a function of tube length b) Experimentally determined HNT sample length distribution.....	60
Figure 5.3: Experimental vs simulated release profiles for dexamethasone a) from 1 μm long 12nm lumen HNTs. b) from 1 μm long 15nm lumen HNTs, c) from 1 μm long HNTs and release profile weighted for different lumen diameters and d) release profile weighted for different lumen diameters and lumen lengths.....	62
Figure 5.4: Release profile of dexamethasone-like particles highlighting the 3 different phases	63

Figure 5.5: a) Release profile for dexamethasone from 15 nm lumen HNTs as a function of temperature. b) Time needed for 90% release of NPs vs temperature. The inset shows the same information but at a scale needed to accommodate the simulation error showing that all points are indeed within the statistical error.....	64
Figure 5.6: Release profiles for dexamethasone from a 15 nm lumen 1 μm long HNTs as a function of temperature.....	66
Figure 5.7: Release profiles of dexamethasone-like particles with zeta potentials from HNTs of lumen 12nm	67
Figure 5.8: Release of dexamethasone like particles for different pH.....	67
Figure A.1: Flowchart of the algorithm used in the model.....	76

ACKNOWLEDGEMENTS

I wish to express my sincere gratitude and appreciation to my advisor, Dr. Pedro Derosa. His guidance, encouragement and trust have supported me throughout all aspects of my doctoral education and research. I would like to thank my committee members: Dr. Yuri Lvov, Dr. Lee Sawyer, Dr. Zeno Greenwood, Dr. Mary Moore, and Dr. Daniela Mainardi for their time and contributions. I am especially grateful to Dr. Yuri Lvov and his research group. I want to thank Joshua Tully and Dr. Elshad Abdullayev for their invaluable help in my research. A number of my fellow graduate students: Joshua Brown, Taylor Tarlton and Andrew Stroud, undergraduate students: Benjamin Beach, Ethan Sullivan and Anil Thapa, and LA-SIGMA RETs and REUs have worked with me on this project and given me useful advice and assistance, and I want to take this opportunity to thank them all. I would also like to thank my friends, Dr. Ilija Pjesic, Dr. Justin Rice, Bilal Dia, Ishan Kamal Khan, Suvashis Thapa, Okoye Chuka, Dr. Ayorinde Hassan, Mary Lee Fair, and my sister, Anusha Elumalai, for making this endeavor and my life, adventurous and fun.

I would be remiss if I did not acknowledge LONI computational resources, which I used extensively. This work was undertaken with financial support from the NSF EPSCoR LA-SigMA project under award #EPS-1003897.

CHAPTER 1

INTRODUCTION AND LITERATURE REVIEW

1.1 Background

Nanotechnology gave scientists a number of materials that enabled the experimental realization of concepts that could previously only be realized as thought experiments. No other nano material has proven more valuable in this regard than nanotubes (NTs). Since their discovery in 1991, carbon nanotubes (CNTs) have attracted considerable interest due to their exceptional mechanical, chemical, optical, and electronic properties that make them suitable for a wide variety of applications including catalysis, electronics, and molecular sensing [1], and of particular interest to this work, molecular storage and controlled release [2-15]. Indeed, there is an increasing amount of ongoing research to produce functional nano containers for their use, among other areas, in biomedical applications, particularly drug delivery [5-7, 16-19]. However, the use of different NTs of various types (not just CNTs) has been proposed beyond the biomedical field. There are therefore several motivations to develop controlled release systems.

Conventional encapsulation approaches, based on bulk emulsification, have significant limitations on their applicability as these methods achieve only limited encapsulation efficiency, thereby wasting valuable active agents [1]. To overcome the shortcomings of conventional approaches and achieve advanced functionalities, effort

has to be made into designing, understanding, and implementing nano carriers [2]. There has been a lot of interest in using nano materials to develop sustained release vehicles to deliver active cargo such as proteins [1, 3, 4], cells [5, 6], drugs [7, 8], anti-corrosives [9], and other such agents at specific sites at a controlled rate either in response to an external stimuli or continuously over time in a zero order release. There are various potential candidates for such carrier vehicles like nano particles (self-assembled or otherwise) [10, 11], porous materials (porous silicon and meso-porous silica)[12-15], soft drug delivery systems (micelles, liposomes, emulsions, emulsion drops) [16-22], capsules (nano-gels, polymer hydrogels and polymer complexes) [23-26], and micro and nano cylinders - nanotubes (functionalized, single and multi-walled).

1.2 Nanotubes

Microcylinders and nanocylinders are an interesting geometry for the encapsulation and release of active agents [27]. Micro/Nano cylinders or tubules range in size from 1000 μm to a 1-2 nm. From carbon nanotubules, lipid tubules in the submicron regime, to hollow or porous polymers or glass in the millimeter range. Even though some of these systems have high loading capacities, they have release mechanisms that are difficult to regulate. Every application requires specifically designed carriers to fully achieve its goals. For example, in drug delivery applications, the size of a vehicle is critical as it determines the ability to pass through a narrow channel in an organ, and its shape is important for determining the interactions among vehicles and cells [28]. The targeted delivery and stimulated release of drugs at a desired rate are very important for maximizing the effects of a drug [2, 15, 16, 29]. Among the various potential candidates for such carriers, certain nanotubes like halloysite nanotubes(HNTs), CNTs, and

lipid nanotubes rank highly due to their unique physical, chemical, and physiological properties [30].

While CNTs have very interesting physicochemical properties such as an ordered structure with high aspect ratio, light weight, high mechanical strength, and high surface area [30], they have been limited to no applications as drug delivery vehicles due to their cytotoxicity. Nanotube-based nano carriers provide for the dynamic encapsulation and release of materials [7, 29-33]. Indeed, there is an increasing amount of ongoing research to produce functional nanometer-scale containers at the time that there is growing demand for their use, among other areas, in biomedical applications, particularly drug delivery [31-37]. However, the use of different NTs of various types (not just CNTs) has been proposed beyond the biomedical field in a variety of applications such as the controlled release of anti-corrosives [38, 39], water purification [40], polymer composites [41, 42], and antimicrobial coatings [43]. All of these applications serve as motivations for developing controlled-release systems, which besides improving systemic availability, alter the temporal and localization release patterns and availability of molecular species of interest.

For instance, NPs can be incorporated into nano carriers that have access to the whole systemic circulation, but are delivered less rapidly than free NPs. Nanotubes can effectively protect entrapped drug molecules against denaturation or degradation over the delivery process [44]. Furthermore, nanotubes have large inner volumes that can allow for loading of more than one therapeutic agent [45]. Last, but not least, some nanotubes like HNTs have separated inner and outer surfaces, which can be differentially functionalized to load the desired molecules, but impart chemical features to the

outer surface allowing for site-specific drug delivery [46]. The combination of these characteristics makes nanotubes a unique material with the potential for diverse applications, including fundamental studies of biological systems, drug delivery, tissue engineering, molecular sieves [47], nano-test tubes [48], hydraulic actuators [49], hydrogen storage [50], selective catalysis chemical sensors [51], biosensors [52, 53], and molecular/ion channels [54-56].

The adaptation of HNTs for entrapment and controlled release was the result of the work of Burke and Singh [57]; Price *et al.* [58] reported the entrapment of oxytetracycline HCl in copper coated microcylinders utilized in antifouling coatings for delivery of hydrophilic and hydrophobic active agents [59]. Price *et al.* [58] also reported the use of microcylinders for the delivery of proteins and growth factors.

1.3 Controlled Release

When designing controlled-release systems, it is important to identify and understand particular mechanisms involved in the release process. Often, more than one mechanism is involved at a given time or different mechanisms may dominate at different stages of the NP delivery process. There are several modes of controlled NP delivery, and it is important to study and identify associated mechanisms. Among the many applications this work focuses on a particular area of interest: smart sustained-release delivery systems. A sustained release dosage form can overcome the problem of the need for frequent intake of medication for it to be therapeutically effective [60]. Such a dosage form normally contains the drug dose required to maintain a therapeutic concentration of the drug in the body for the needed durations [60]. With most drugs there is a high risk if dose-dumping occurs. Dose dumping is the release of the entire dosage in a short span of

time and can cause severe and sometimes lethal side effects [60]. The probability of dose dumping is dependent on the environment surrounding the delivery container [60].

1.4 Diffusion

Nanochannels, nanopores, and nanotubes can be treated as porous media and the movement of fluid through them can then be described as diffusion through a porous material. Diffusion is a very important component of many controlled-release systems. All molecules constantly undergo random collisions with other molecules. Molecules in nanotubes, therefore, undergo constrained random thermal motion. At any step, the direction of motion of a molecule is random, and it repeatedly changes due to collisions with other molecules. Over time, the displacement of the molecule from its point of origin is the result of a multitude of such random steps. Macroscopically, the independent random walks taken by a large number of drug molecules lead them from regions of higher concentration to regions of lower concentration. Thus, diffusion of a substance occurs down its concentration gradient.

The mechanism of diffusion through pores is further classified as Knudsen diffusion [61, 62], molecular diffusion [63], surface diffusion [64], and hydrodynamic flow [65]. Diffusion is classified as Knudsen diffusion when the mean free path of the fluid is of the order of magnitude of the channel's size. In this case, diffusion is governed by the collisions of molecules with the channel wall. Knudsen diffusion occurs in nano systems where the diameter of the channel is only a few times the molecular diameter of the fluid, and the ratio of the channel diameter to the mean free path of the molecules is less than 0.2 [61, 66]. When the diffusion is dominated by inter particle/molecular collisions, the diffusion is called molecular diffusion [63]. When the fluid is adsorbed to

the channel surface and diffuses along the surface, the diffusion is called surface diffusion [64]. Hydrodynamic or Poiseuille flow occurs due to the presence of a pressure gradient [65]. Essentially, diffusion can be broadly classified as either self-diffusion (the motion of the molecules in absence of a gradient) or transport diffusion (the motion of the molecules due to a concentration gradient) [67, 68].

Many predictive theories have also been applied to understand the diffusion of particles along the surface and through the pores at the ends of the nanotubes, and through the surrounding media [69-73]. One approach has been to employ classical diffusion theory, which neglects velocity effects, but this approach shows discrepancies in the early stages of particle motion [70]. In nanotubes the effect of the wall on the motion and the restrictions they impose have to be considered [74, 75]. The initial condition of the system and the boundary conditions play important roles. The dynamics of a particle are determined based on the variations in the total energy of the system.

When the interaction between the encapsulated particles and the wall is repulsive, diffusion is down the center, whereas when the wall-particle interaction is attractive, diffusion is along the wall. The model is valid for channel sizes larger than the diameter of the particles. In nano scale molecular channels as described in [72, 73], site to site hopping describes the motion of the particle motion better than continuous diffusion paths. The behavior of the diffusing species in the nano regime differs from macro scale systems and as the complexity of the system increases, it gets smaller. Several factors, some of which are neglected while simulating larger systems like the electro kinetics, viscous heating [76], and surface forces like van der Waals, electrostatic forces, steric forces and gas surface properties start playing dominant roles [77, 78]. Diffusion through

nano channels is generally modeled using either direct simulation Monte Carlo (DSMC) or the MD approaches [69, 70, 72, 77].

The continuum approach is used for many applications, and it is based on finding the macroscopic properties of the media the nanotube is immersed in (the permeate) [79]. In the nano regime there is a marked departure in behavior from the predictions of the continuum approach with no-slip boundary conditions [66]. To characterize this departure from the continuum regime, the Knudsen number k_n , which is defined as the ratio of the mean free path to the characteristic length scale, is used. Tsien *et al.* [80] in their work further classified diffusion based on the value of the k_n into continuum flow for $k_n < 10^{-3}$, the somewhat rarefied slip flow regime with $10^{-1} > k_n > 10^{-3}$, the intermediately rarefied transition regime with $10 > k_n > 10^{-1}$, and the highly rarefied free molecular regime with $k_n \geq 1$ [81]. The continuum flow regime can be accurately described by the Navier-Stokes equations with appropriate boundary conditions. The Navier-Stokes equations with appropriate partial slip boundary conditions also describe the slip flow regimes. The Boltzmann equation (no collisions) accurately models free molecular flow.

Diffusion in nanotubes occurs in the region with $k_n \geq 10^{-1}$ and can neither be totally described by molecular flow nor can they be described by totally continuum flow since the characteristic length is equivalent to the mean free path and rarefaction effects cannot be ignored any longer [76, 77]. This is further illustrated by Arkilic *et al.* and others [77, 78, 80, 82] in their papers in which they studied the flow of low Reynolds number (Re) gases through the micro channels. DSMC method is used extensively nowadays to investigate gas diffusion in micro geometries [81, 83]. However this method

has limitations in that it requires a large number of particles to be accurate, and this is expensive in both computational time as well as memory requirements, especially for the low-speeds in nano devices [82]. A prerequisite for DSMC is that the time steps need to be smaller than the collisional time scale. For a moderately practical system this translates to extremely expensive computational resources, thereby limiting the use of DSMC to solve small-scale problems.

DSMC simulations are further limited by the fact that for high aspect ratio geometries (micro and nano channels) a minimum of 500,000 cells are required [84]. The error in DSMC is inversely proportional to the square root of the number of simulated particles; therefore, decreasing the number of particles in the computational cell increases the error in the solution [76]. While there are quite a few methods to describe the slip flow regime, the diffusion in the transition regime are studied using MD and other statistical methods [69, 74, 76, 85]. The free molecular approach like MC and MD considers the fluid to be a collection of discrete particles [69, 85]. This can be modeled using either deterministic [74] or statistical approaches [72], both of which are capable of providing the position and energy of all the individual molecules at all times.

The molecular approach utilizes a Boltzmann distribution (at a given temperature), which is ideal for predicting small-scale interactions in this regime to evaluate individual particle dynamics. The evolution of particle positions is obtained by numerically integrating Newton's equations of motion. The choice of the potential is arbitrary. Notwithstanding the theoretical relevance of MD models for modeling small-scale interactions, it is unfeasible to simulate a realistic nano flow problem using present day supercomputers. Most MD calculations are limited to femtosecond time steps

required to represent fast vibrations occurring in molecules, thereby limiting the results to short time scale (picoseconds to nanoseconds) phenomena [69, 74]. A one second real time simulation of transition flow is expected to take thousands of years of CPU time using MD [80]. MD is computationally expensive probabilistic models like DSMC provide accurate solutions as the time step decreases and the number of particles in the cell is sufficiently large. Both MD and DSMC have extremely slow convergence rates compared to continuum models. As an alternative, higher-order extended or generalized hydrodynamic equations have been proposed which perform equally well in both the continuum and slip/transition regimes [77]. The Burnett equations represent a second order correction to the equilibrium distribution function of gas diffusion [86]. Fubing *et al.* [87] used the Burnett equations to study gaseous diffusion in micro/nano channels. A pressure driven plain Poiseuille flow, backwards facing step flow and flow through filters were modeled. But their study was limited to two-dimensional cases. The Burnett equations are numerically unstable, which implies that convergent results in Poiseuille flow can only be obtained at small Kn [86].

The diffusion behavior of the NPs confined in the nanotubes in a liquid or gaseous media is dependent on the surface chemistry of the nanotube and the NPs, and has been found to be crucial for effective encapsulation of the NPs in nanotubes and their controlled release [15]. However, due to the lack of suitable instruments, it is still a big challenge to carry out experiments to investigate the diffusion behavior of the NPs in nanotubes in details. Fortunately, simulations can be utilized to study the diffusion/flow behaviors in the nanotubes. Computational studies of the mechanism of diffusion through nanotubes and nanopores have begun fairly recently and the work done in this field is

described here. Mao and Sinnott [74] studied the self-diffusion of methane, ethane and ethylene through SWNT of various diameters and helical structure at room temperature.

They also studied the diffusive flow of binary mixtures of methane and ethane, methane and *n*-butane, and methane and iso-butane through SWNT's using MD. Düren *et al.* [88] computed the transport diffusion coefficients for CH₄ & CF₄ mixture in multi-walled carbon nanotubes with three layers with an innermost lumen diameter of 2.978 nm. Sholl *et al.* [89] studied the diffusion of gases like SnBr₄, Ar, Kr, Xe, SF₆, SnCl₄, CH₄, CF₄, CCl₄, and Ne through AlPO₄-5 molecular sieves. Keffer [90] carried out MD diffusion studies of methane and ethane in a 1D molecular sieve of AlPO₄-5 to study the temperature dependence of the diffusivities of the constituents of a binary adsorbed mixture. Simulations were performed to study the transport of these species as single adsorbed species and binary mixtures. Nicholson [91] investigated the transport selectivity of CH₄ and CO₂ through cylindrical carbon pores with walls that were structureless. Tuzun *et al.* [92] studied the flow of Helium and Argon through carbon nanotubes to study the effect of the rigidity of the tube on the behavior of the fluid using MD. Seo *et al.* [93] used a dynamic Monte Carlo simulation to calculate transport diffusion of hydrogen and hydrocarbons in nano porous carbon membranes with slit-like pores. Ten Bosch used Brownian dynamics to study the wall effects and time dependent particle concentration induced flow in adsorbing nanopores [94].

As a means of achieving numerically effective small-scale diffusion predictions with reasonable computational time, a Monte Carlo based model for small flow applications has been applied to diffusion simulations through nano-geometries and nanopores. These studies consider the slip and transition regimes with $10 > k_n \geq 10^{-1}$.

The aim of this work is to help develop systems which enable active agents to be encapsulated, targeted to a specific region and released “on demand” in response to an external stimulus. Such systems provide a means of controlling the NP concentration and reducing the risk of reservoir depletion.

1.5 Halloysite Nanotubes

Due to the toxic nature of CNTs, researchers look with interest into more natural options like clay. Most common clay structures possess a nano-layered morphology, for example, kaolin and montmorillonite [95], while other naturally occurring nanoclays show a hollow tubular structure [32, 95]. Two such promising nanoclays that can be used as nano containers with controlled release properties are Imogolite nanotubes (INTs) [95] and natural Halloysite nanotubes (HNT) [32, 96]. INTs, however, present some level of toxicity [97]. HNT clay is a two-layered aluminosilicate, chemically similar to kaolin, with a hollow tubular structure in the sub-micrometer range. HNT is abundant, durable, and biocompatible; furthermore, it is cheap compared to synthetic nanomaterials with similar morphology. HNT is formed naturally when kaolin sheets roll up on themselves [96]. Kaolin sheets are rolled into tubes because of the strain caused by a lattice mismatch between adjacent silicon dioxide and aluminum oxide layers [96].

As with most naturally occurring materials, HNTs size varies from HNT to HNT in a batch, and the external diameter varies from 50 to 70 nm with lumen inner diameters from around 5 nm to as large as 40-50 nm [96]. The length of HNTs varies from 0.5 - 1.5 μm . HNTs have a specific density of 2.53 g/cm^3 , a refractive index of 1.54, a pore volume of 1.25 mL/g, and a specific surface area of $65 \text{ m}^2/\text{g}$ [96, 98]. The outer surface of the HNTs has properties similar to SiO_2 with negative charge at pH 6 – 7 while the inner

cylinder core is Al_2O_3 , which is positively charged for a pH of less than 8.5 [99-101]. The positive charge of the inner lumen promotes loading of HNTs with negative macromolecules within void spaces, while at the same time they are repelled from the negatively charged outer surfaces [96, 99-101]. HNTs are capable of entrapping a range of active agents within the inner lumen, followed by their retention and slow release.

Price *et al.* [6, 7] and Levis and Deasy [8, 9] were pioneers in studying the loading and release behaviors of various pharmaceuticals (e.g. dexamethasone) from HNTs. HNTs lumen produce a large capillary force in polar liquids which helps in loading NPs within the tubes. At pH above 2.5, HNTs have a negative SiO_2 outer surface with an electrical zeta-potential of -35 mV. This allows for its good dispersibility in water, alcohol, acetone, and polar polymers. Control over loading and release has been achieved using several methods such as silanization of lumen to increase the hydrophobicity of the inner tube for higher adsorption of low water soluble drugs [6, 7], lumen enlargements by etching [6, 7], and tube encapsulation by the formation of polymeric coating and caps at the tube's ends [6, 7]. It has been shown that loading efficiency can be increased up to 30 weight % with lumen enlargement using acid etching of the internal alumina [8].

These modified HNTs can be loaded with drugs at 10–30 weight % and used for sustained release of chemical agents [1, 3, 5, 8–11]. HNTs are biocompatible as was demonstrated on different cell cultures and micro worms [2, 12, 13]. While the biocompatibility of halloysite has been confirmed [10], its medical use might be restricted to oral dosing, dermal application or dental uses [10], due to the non-biodegradability of the aluminosilicate. Consequently, increasing attention is now being

paid to the usage of halloysite as a substrate for the loading and sustained release of agrochemicals (herbicides, pesticides and fertilizers) [10, 11], anticorrosion agents [10, 12] and bio-actives agents (e.g. enzymes) [1, 13–15]. Surface chemistry, tubule morphology, submicron size and biocompatibility make this nanomaterial an excellent candidate for nanopore-controlled release of antiseptics, drugs, and proteins with delivery times of a few hours to several hundred hours [8–10]. Halloysite nanotubes provide good encapsulation for chemicals allowing longer release time. Larger and precisely controllable release times are important for application like smart halloysite–polymer composites and can be accomplished by synthesizing the tube's end stoppers. It has been shown that stoppers are effective at extending the release time of corrosion inhibitors and drugs [16–17].

The adaptation of HNT microtubules for controlled release was the result of the work of Burke and Singh [57]. HNTs were found to be a viable and inexpensive nanoscale container for encapsulation of drugs and other NPs [32, 35, 101-110]. This was first demonstrated by Price, Lvov, and Kelly [33, 111, 112]. HNTs physiochemical characterization as a novel drug delivery system was also reported by Levis *et al.* [34, 36]. HNT's strong surface charge has been exploited by Lvov *et al.* [32, 33, 35, 53, 96, 101, 102, 105-107, 110, 113-116] for the design of a nano-organized multilayer using layer-by-layer assembly and for use in sustained release experiments. An *in vivo* drug delivery system using HNT for the treatment of periodontitis has been demonstrated in studies by Kelly *et al.* [37]. Lvov *et al.* [101, 117] reported the entrapment of oxytetracycline HCl in copper coated microcylinders utilized in antifouling coatings for delivery of hydrophilic and hydrophobic active agents. Price *et al.* [35] reported the use

of microcylinders for the delivery of proteins and growth factors.

To further delay/control the release, CdS and Fe₃O₄ NP have been used as end caps for HNTs to regulate the opening/closing of the pore entrance of meso-structured materials [118]. The covalent modification of the inner surface of HNT, to be able to incorporate more ferrocene than pristine nano clay, was reported by Cavallaro *et al.* [119]. Cavallaro *et al.* [119] also reported the modification of HNT lumen by incorporating perfluoroalkylated anionic surfactants to obtain stable colloidal dispersions in water with enhanced oxygen solubilization ability. Biocompatible HNT-based fluorinated surfactants have been proposed as oxygen carriers in biomedical applications [120]. Finally, the possibility to adjust the HNT's inner diameter between 15 and 30 nm, by selective etching, while maintaining the outer diameter unchanged, was demonstrated in reference [121].

Therefore, experimentalists, could have short ca 0.5 μm (milled HNT) and long 1-1.5 μm clay nanotubes with an inner diameter between 15 to 30 nm, can vary the inner and outer surface potential of HNTs by adsorption of charged molecules, and are empirically trying to optimize these parameters to have controlled sustained release without the possibility to predict and optimize these tubule carrier properties [96]. The ability to simulate the process can certainly assist in this task.

1.6 Motivation

Experimentalists are empirically trying to optimize these parameters to have controlled sustained release without the possibility to predict and optimize these tubule carrier properties [2]. The ability to simulate the process can certainly assist in this task.

When designing controlled-release systems, it is essential to ascertain and comprehend particular mechanisms involved in the release process. Even though different mechanisms dominate at different stages of the NP delivery process, each stage may have more than one mechanism acting at the same time. The past decade represented a period of concerted experimental and theoretical research efforts to elucidate several of the hitherto incompletely understood aspects. The need to control the release rates accurately and be able to predict controlled delivery/release characteristics consistently, such as release times, motivates this research. Thus this paper highlights controlled delivery from HNT by modeling the associated interactions between the HNTs and the NPs. To achieve optimal release profiles for a given set of initial and boundary conditions, like initial molecular concentration or pH and temperature of the surrounding media, only a few simulations parameters need to be tested. The results obtained from the simulations can then be translated to the experiments which in turn can produce the necessary data to calibrate and validate the computational models.

When designing controlled-release systems, it is important to identify and understand particular mechanisms involved in the release process. Often, more than one mechanism is involved at a given time or different mechanisms may dominate at different stages of the NP delivery process. The past decade represented a period of concerted experimental and theoretical research efforts to elucidate several of the hitherto incompletely understood aspects. The need to control release rates accurately and be able to predict controlled delivery/release characteristics consistently, such as release times, motivates this research, thus this work highlights controlled delivery from HNT by modeling associated interactions between the HNTs and the NPs. To achieve optimal

release profiles for a given set of initial and boundary conditions, like initial molecular concentration or pH and temperature of the surrounding media, only a few simulations parameters need to be tested. The results obtained from simulations can then be translated to the experiments which in turn can produce the necessary data to calibrate and validate the computational models. In the next section, the model developed for this work is presented, then the results are described with appropriate discussions of the virtues and limitations of the model, and finally conclusions are offered.

1.7 HNTs with Endcaps

A number of experimental techniques can be used to form the end caps at the end of an HNT ends. In one of those techniques, HNTs are exposed to urea-formaldehyde pre-polymer solution. Rapid cross-linking of the pre-polymer causes the formation of a thin polymer shell that also plugs the tube's endings. Another approach consists of the formation of copper-inhibitor clogs due to the chelation of Cu (II) ions [18]. Corrosion inhibitors form 2D polymer films that cover the entire HNT surface and effectively seals the tube's endings and any other leakage defects. HNTs are rinsed with CuSO_4 solution for a few seconds for the formation of the stoppers and the removal of extra material.

Starch stoppers at HNT's ends is another option. These stoppers are formed by mixing halloysite with starch and heating it at 200°C in a thermal reactor. However, this method cannot be used for proteins and drug encapsulation due to the high temperatures involved. The fourth approach is to form a thin coating on the halloysite's external surface through sequential adsorption of the film-forming components A and B. A is an insoluble film forming compound and B is a complexation compound that covers the entire surface of the HNTs and clogs the tube's openings and any other defects.

Alternatively, component A may be loaded into the HNT lumen and then the tubes may be rinsed with component B.

Another approach is to encapsulate HNTs via polymer deposition. This method was demonstrated for release of diltiazem-HCl in reference [19]. Coating with chitosan and poly (ethyleneimine) reduces the release rate of diltiazem 2–3 times. Further cross-linking the HNTs with glutaraldehyde provides additional retardation in the release; however, this method also significantly reduces the loading efficiency of the HNTs [19].

Having a negative surface, HNTs can be effectively coated by sequential adsorption of positively and negatively charged polyelectrolytes (layer-by-layer, LbL-technique). Polycation / polyanion multilayers form a shell on the halloysite providing a diffusion barrier and slowing down the release. HNTs readily adsorb polycations, such as chitosan, polyethyleneimine (PEI), polylysine or polyallylamine hydrochloride (PAH), forming a thin positively charged layer on the surface. Then negatively charged polyelectrolytes, polystyrene sulfonate (PSS), polyacrylic acid (PAA), or heparin can be deposited to form a strong polycation/polyanion complexation. Such LbL coating allows inverting halloysite surface potential to be positive [20].

Immobilization of proteins, DNA and other biopolymers on HNTs were also demonstrated [20, 21]. Coating HNTs with large molecular weight polyelectrolyte shells allowed for a decrease in the release rate of dexamethasone drug from 6 hours to 15 hours. The release profiles were significantly affected by the type of polyelectrolytes used to generate the shell [20]. Coating HNTs with thicker stoppers at the tube's ends was achieved by the interaction of triazoles and imidazoles with transition metal ions. These complexes form thin films which cover the entire external surface of the HNTs

also forming stoppers at the tube's ends [22]. Such coated halloysite may contain loaded chemical with a much longer release (e.g. corrosion inhibitors and antifouling agents) and may be doped into polymers to provide additional functions [6, 7, 9, 14].

Chapter 4 of this work highlights controlled delivery from HNT by modeling associated interactions between the HNTs, the end caps, and the NPs. Here, the model is extended to include porous end caps and the release profile as a function of end caps characteristics is described. In the next section, the model developed for this work is presented, then results are described with appropriate discussions of the virtues and limitations of the model, and finally conclusions are offered.

To understand the interaction of nanoparticles on a molecular level, calculation of interaction potential is of great importance. However, different states of the system are separated by high barriers which impede the exploration of phase space to obtain a valid average force on the particles. There exist various methods which have been proposed for efficient calculations of interaction potentials by applying different strategies to try to better sample the phase space.

In chapter 5 of this work, the interactions of dexamethasone (our NP of interest), with the inner lumen wall of HNTs, with respect to HNT length, temperature and pH is investigated. Experimental observations show that dexamethasone can be taken as a non-polarizable entity, and it is pretty hydrophobic. Therefore, the typical tendency of the dexamethasone molecules is to evade the water and sticks to the walls. We can subjugate the shielding due to the media by using an adaptive biasing method which corrects the total potential experienced by an NP in the HNT.

In chapter 6 we offer conclusions and summarize the results of the effect of different parameters like temperature, pH, HNT size and NP size on the release of the NPs from the HNTs.

In chapter 7 we offer two possible uses of our research namely the diffusion of NPs through concrete pores and the study of diffusion through hydrogels.

In the next section, the model developed for this work is presented, then the results are described with appropriate discussion and finally conclusions are offered and suggestions made for possible future work.

CHAPTER 2

METHODOLOGY

2.1 Model and Simulation Method

Nanometer-scale tubules of HNT introduce the prospect of observing purely non-Knudsen transport (because the radius of the nanotube is around 15 nm) at atmospheric pressure and temperature. Here, we present a rather unique 3-D coarse grain Monte Carlo (time –quantified) model that uses the classic kinetic theory coupled with Guy-Chapman-Enskog theory and Poisson-Boltzmann theory to describe the molecular transport in HNT channels and highlights the role of surface effects on molecular diffusion to determine transport efficiency. This model uses several basic assumptions about the nature of molecules, molecules–wall interactions, and the influence of collisions on the NPs' displacement. It is proposed that the model can be used as is in other types of nanoporous channels as long as the channel's wall can be considered smooth, rigid, and defect free. With minor modifications, less uniform wall surfaces can also be modeled.

For sufficiently large cylindrical structures (pores or nanotubes), in the 50–100 nm range (e.g. HNTs), investigation can focus on the interaction of the permeate with the inner charged surface of the NT. SEM and STM images of HNT and a schematic of the cylindrical nanotube are shown in Figure 2.1.

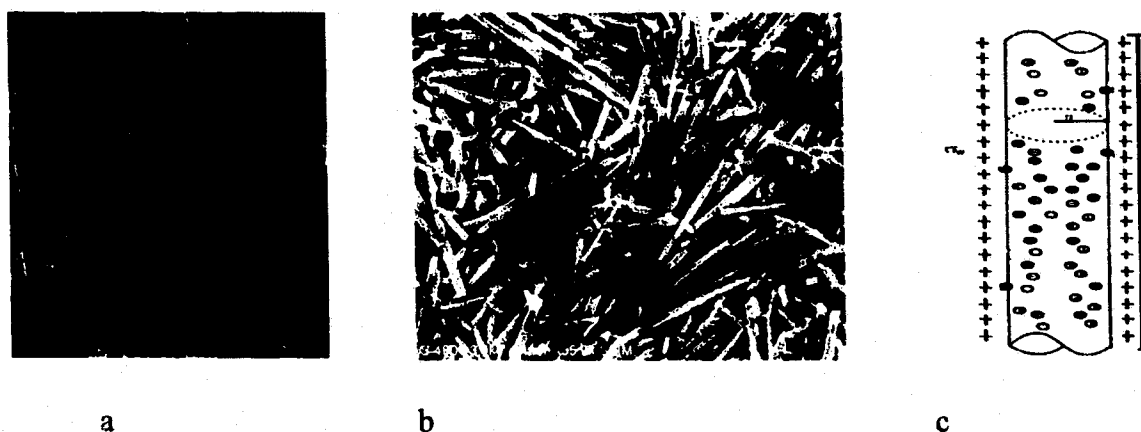


Figure 2.1: a) TEM and b) SEM images of a clay nanotube batch, c) Schematic cross section of a charged cylindrical nanotube with ions inside used as a model for this work.

The model, implemented by utilizing MATLAB [122], was designed to simulate NP diffusion in long, defect free NTs and out of the ends of the NTs. The hydrodynamic radius, the effective radius of a hydrated NP in the solution, is considered in these simulations, rather than the actual gas phase radius. NPs are considered to be spherical in shape and are initially distributed uniformly throughout the cylindrical channel except at the tube's ends where the density is larger to account for the experimentally observed initial burst (see below for more details) with the media in the channels being either a dielectric vacuum. The NP's motion is simulated as a random walk to sample the configuration space subject to interactions among NPs and between the NPs and the HNT walls. Particles are moved one at a time in an arbitrary direction and an arbitrary length up to an upper limit that depends on the kinematics of the system. The move is allowed as long as it is energetically viable and there is no overlap with the walls or with neighboring NPs along the line connecting the initial and final position of the NP. A move is considered energetically viable if the total energy of the system is either reduced or stays the same. If the energy increases, however, the move can still be accepted with

Boltzmann probability. A simulation step is the event where every particle in the system has either moved or attempted to move once.

2.2 NP-Wall Interaction

The NPs are modeled as soft core spheres with hydrodynamic radius R and a zeta potential (the potential at R). The NT's walls are positively charged with a pH-dependent surface charge density. Due to the structure of the HNTs, a soft wall composed of Lennard Jones (LJ) atoms is chosen accordingly. Thus, the ion-wall interaction consists of a coulombic plus a van der Waals (VdW) term with a cutoff for the VdW interactions set to $6R$. The total energy of the system is given by

$$u(r) = \begin{cases} u_{VdW} + u_{CB} & r < 6R \\ u_{CB} & r > 6R \end{cases}, \quad (2.1)$$

where u_{CB} is the energy contributions due to Coulombic interactions and u_{VdW} are the contributions due to VdW interactions.

The VdW ion-wall interaction can be computed by integrating the VdW potential over the wall surface. An analytical expression for the VdW experienced by small charges inside a cylindrical nanotube is given by Afansiev *et al.* [123] as Equation (2)

$$u_{VdW} = -\frac{c_3}{x_0^3} \mu, \quad (2.2)$$

where x_0 is the distance from the wall along a radius and $c_3 = \frac{\langle d^2 \rangle (\epsilon_c - \epsilon_r)}{12(\epsilon_c + \epsilon_r)}$ is the VdW constant. d is the average dipole length, while ϵ_c and ϵ_r are the permittivity of the wall and the media, respectively. In this work $c_3=0.04$ and μ is

$$\mu = \frac{2x_0^3}{\pi} \int_0^\infty \sum_{m=-\infty}^\infty \frac{K_m(kR)}{I_m(kR)} X \{I_{m-1}^2(kr) + 2I_m^2(kr) + I_{m+1}^2(kr)\} k^2 dk, \quad (2.3)$$

where $K_m(x)$ and $I_m(x)$ are modified Bessel functions, with r the distance between the center of the NP and the center of the nano channel, which accounts for the curved shape of the cylinder wall. For further details see reference [123].

The Columbic interaction between the NP and the inner surface of a HNT lumen in a solvent is considered here to correspond to that of a charged spherical NP with the inner part of a charged cylinder of infinite length, except when the particles are at the ends of the tube (for the solution at the ends see below). Utilizing a basic model of electrolyte, the solvent is treated as a uniform background with a dielectric constant containing charged spheres.

Equation (7) describes the potential energy landscape for a charged NP with electrical potential ψ_p in a charged, very long, hollow dielectric cylindrical channel with surface potential ψ_w immersed in a medium of relative permittivity ϵ_r . This is obtained by solving the linearized Poisson-Boltzmann equation for the cylindrical nanotube immersed in a medium of uniform dielectric [124, 125].

In cylindrical coordinates the Poisson Boltzmann equation is

$$\frac{d^2\varphi}{dr^2} + \frac{d^2\varphi}{dz^2} = \frac{1}{\lambda_D} \sinh(\varphi) - \frac{1}{r} \frac{d\varphi}{dr}, \quad (2.4)$$

where λ_D is the Debye length and φ is the potential. The boundary conditions for the charged sphere and the cylindrical lumen of the HNT are $\varphi = \psi_p$ at the particle surface and $\varphi = \psi_w$ at the inner surface of the cylinder's wall. ψ_w in turn depends on the pH of the system which implies that the surface charge density depends on the pH of the medium. The variation of zeta potential (ζ_{HNT}) with pH for HNTs has been published by Lvov *et al.* [113].

The remaining boundary conditions are:

$$\frac{d\varphi}{dr} \Big|_{r=0} \rightarrow 0 \quad \text{and} \quad \frac{d\varphi}{dr} \Big|_{r=R_0} \rightarrow \frac{4\pi}{\epsilon_0 \epsilon_m} q_p, \quad (2.5)$$

where,

$$q_p = \frac{\epsilon \epsilon_0 kT}{\lambda_D e v} \left(\sinh \left(\frac{1}{2} \psi_p \right) + \frac{4\lambda_D}{R} \tanh \left(\frac{1}{4} \psi_p \right) \right). \quad (2.6)$$

Solving Eq. (2.5) gives us the Columbic interaction energy, given by Eq. (2.7)

$$u_{CB}(r) = \frac{\pi \epsilon R \psi_w^2}{\sqrt{1 - \frac{R}{R_0}}} \left\{ \left(1 + \frac{\psi_p}{\psi_w} \right)^2 \ln \left[\left(1 + \exp \left(-\frac{R}{\lambda_D} \left(\frac{R_0}{R} - 1 \right) + \frac{r}{\lambda_D} \right) \right) \left(1 + \exp \left(-\frac{R}{\lambda_D} \left(\frac{R_0}{R} - 1 \right) - \frac{r}{\lambda_D} \right) \right) \right] + \left(1 - \frac{\psi_p}{\psi_w} \right)^2 \ln \left[\left(1 - \exp \left(-\frac{R}{\lambda_D} \left(\frac{R_0}{R} - 1 \right) + \frac{r}{\lambda_D} \right) \right) \left(1 - \exp \left(-\frac{R}{\lambda_D} \left(\frac{R_0}{R} - 1 \right) - \frac{r}{\lambda_D} \right) \right) \right] - \frac{A}{24\pi \epsilon \lambda_D \psi_p^2} \frac{2 \frac{R}{\lambda_D} \left(\frac{R_0}{R} - 1 \right)}{\left(\frac{R}{\lambda_D} \right)^2 \left(\frac{R_0}{R} - 1 \right)^2 - \left(\frac{r}{\lambda_D} \right)^2} \right\}, \quad (2.7)$$

in this implementation, ψ_p was represented by ζ_p , which is consistent with the NP's radius being the hydrodynamic radius R . R_0 is the HNT radius, r is the radial distance between the axis of the cylinder and the NP, λ_D is the Debye length and A is calculated using Equation (8)

$$A = \frac{3}{4} kT \left(\frac{\epsilon_w - \epsilon_m}{\epsilon_w + \epsilon_m} \frac{\epsilon_p - \epsilon_m}{\epsilon_p + \epsilon_m} \right) + \frac{3hV_e}{8\sqrt{2}} \frac{(n_w^2 - n_m^2)(n_p^2 - n_m^2)}{\sqrt{(n_w^2 + n_m^2)(n_p^2 + n_m^2)} \sqrt{(n_w^2 + n_m^2) + (n_p^2 + n_m^2)}}, \quad (2.8)$$

where ϵ_w is the permittivity and n_w is the refractive index of the HNT wall, ϵ_p is the permittivity, n_p is the refractive index of the NPs, and ϵ_m is the permittivity while n_m is refractive index of the surrounding medium. At the HNT entrance, the infinity tube approximation is discarded in favor of the interaction between the NP and a rounded HNT pore entrance as schematically represented in Figure 2.2 [126].

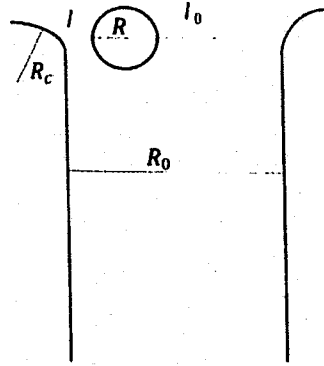


Figure 2.2: Geometry considered as a model for this work.

Eq. (2. 10) describes the potential energy landscape for this situation [124, 125].

The boundary conditions here are

$$\frac{d\varphi}{dr} \Big|_{r=0} \rightarrow 0 \quad \text{and} \quad \frac{d\varphi}{dr} \Big|_{r=R_c} \rightarrow \frac{4\pi kT}{\epsilon_0 z e} \varphi \Big|_{r=R_c}, \quad (2.9)$$

which implies,

$$u_{CB}(r, z) = \frac{\pi \epsilon R \psi_w^2}{\sqrt{(1+\frac{R}{R_c})(1-\frac{R}{R_0+R_c})}} \left\{ \left(1 + \frac{\psi_p}{\psi_w}\right)^2 \ln \left[\left(1 + \exp\left(-\frac{l}{\lambda_D}\right)\right) \left(1 + \exp\left(-\frac{l_0}{\lambda_D}\right)\right) \right] + \right. \\ \left. \left(1 - \frac{\psi_p}{\psi_w}\right)^2 \ln \left[\left(1 + \exp\left(-\frac{l}{\lambda_D}\right)\right) \left(1 + \exp\left(-\frac{l_0}{\lambda_D}\right)\right) \right] - \frac{A}{24\pi\epsilon\psi_p^2} \left(\frac{1}{l} - \frac{1}{l_0}\right) \right\}, \quad (2.10)$$

where R_c is the radius of the pore rounding, and

$$l = R \sqrt{\left(\left(\frac{R_0+R_c}{R} - \frac{r}{R}\right)^2 + \left(\frac{R_c}{R} + \frac{z}{R}\right)^2\right)} - R_c - R, \quad (2.11)$$

$$l_0 = R \sqrt{\left(\left(\frac{R_0+R_c}{R} + \frac{r}{R}\right)^2 + \left(\frac{R_c}{R} + \frac{z}{R}\right)^2\right)} - R_c - R. \quad (2.12)$$

2.3 NP-NP Interaction

The interaction energy between two ions is expressed as

$$U(r_{ij}) = \begin{cases} U_{VDW} + U_{CB} & r_{ij} < \lambda_D \\ U_{CB} & r_{ij} > \lambda_D \end{cases}, \quad (2.13)$$

where U_{VDW} is the VdW interactions between a pair of particles accounted for by the 12-6 Lennard-Jones Potential [127] given by Eq. (2.14)

$$U_{VDW} = 4\varepsilon_{ij} \left[\left(\frac{\sigma_{ij}}{r_{ij}} \right)^{12} - \left(\frac{\sigma_{ij}}{r_{ij}} \right)^6 \right], \quad (2.14)$$

where ε_{ij} is the depth of the energy well, σ_{ij} is the distance at which the energy is equal to zero, and r_{ij} is the distance between the 2 particles.

U_{CB} is the screened electrostatic potential for a spherical charged particle of radius R immersed in an electrolyte with positive and negative ions. According to the DVLO theory (named after Derjaguin, Landau, Verwey and Overbeek), the screened potential is given by Eq. (2.15) [128]

$$U_{CB}(r) = \sum_{i,j=1}^N k_B T \lambda_b \frac{q_i q_j e^{\kappa R}}{(1+\kappa R)r_{ij}} e^{-\frac{r_{ij}}{\lambda_D}}, \quad (2.15)$$

where q_i and q_j are the charges of the individual particles, r_{ij} is the distance between the two particles, R is the radius of the molecule, $\lambda_b = \frac{e^2}{4\pi\epsilon_0\epsilon_r k_B T}$ is the Bjerrum length, and λ_D is the Debye length given by Eq. (2.16) [129]

$$\lambda_D = \frac{1}{\sqrt{(8\pi\lambda_b N_A I)}} = \sqrt{\frac{\epsilon_r \epsilon_0 k_B T}{2N_A e^2 I}}, \quad (2.16)$$

where N_A is the Avogadro number, $I = \frac{1}{2} \sum_{i=1}^n c_i z_i^2$ is the ionic strength, where c_i is the molar concentration, z_i is the charge number of the i th ion and e is the elementary charge,

ϵ_r is the permittivity of the medium, ϵ_0 is the dielectric constant of the vacuum, k_B is the Boltzmann constant, and T is the temperature.

2.4 Introducing Time in the Algorithm

The Monte Carlo Algorithm as described above does not provide time correlated sequence of events. Kinetic/dynamic Monte Carlo algorithms have time incorporated explicitly, but they require the process rate to be known.

The approach to introduce time to the algorithm presented here is as follows. The maximum hop distance of the molecules is taken to be the mean free path as described by the Chapman-Enskog theory for fluids and molecular gas flow for Eq. (2.17) [130].

$$\lambda = \frac{16\kappa_c}{5\rho\sqrt{(2\pi RT)}}, \quad (2.17)$$

where R is the gas constant, T is the temperature, ρ is the combined density of the NPs and the permeate inside the NT, and κ_c is given by Eq. (2.18)

$$\kappa_c = (1 + 2.5\phi) \left(\frac{2.6693}{10^6} \frac{\epsilon(mT)^{\frac{1}{2}}}{4r^2\omega K_B T} \right), \quad (2.18)$$

where ϕ is the NPs volume fraction, K_B is the Boltzmann constant, ϵ is the maximum energy of attraction, $2r$ is the collision cross section, and ω is the Chapman-Enskog collision term.

In the ideal case of completely elastic specular collisions in a completely smooth cylinder, molecules will translocate through the NT in a billiard-ball-like series of collisions and the NT would introduce no resistance to transport. In reality, non-bonded interactions among NP and between NP and the tube's wall, as well as surface defects and charges in the NT's openings, can act as scatterers or anchors and randomize the

molecular velocity. Therefore, the mean free path of NPs in the nanotube depends on the nanotube diameter and the average distance between the regions/points inducing scatter. All these factors are accounted for in Equation (17).

In molecular transport, the mean square displacement of transported particles scales nonlinearly with time. This kind of transport is observed in many physical processes and often leads to a broad-ranged particle distribution density, both in space and time. The random walk formalism as implemented here, offers an attractive framework to understand and model such transport. This approach assumes that transition times associated with particle displacements are independent of each other. So the velocity of successive jumps are not correlated.

The velocity of the particles during hops has contributions from thermal velocity and a potential-energy-dependent drift velocity. The average total velocity is given by Eq. (2.20)

$$\bar{v}_{Tot} = \int_{v=0}^{v=\infty} v f(v) dv = 4\pi \left(\frac{M}{2\pi RT} \right)^{\frac{3}{2}} \int_{v=0}^{v=\infty} v^3 e^{-\left(\frac{Mv^2}{2RT}\right)} e^{U/KT} dv, \quad (2.19)$$

$$\bar{v}_{Tot} = \sqrt{\frac{8RT}{\pi M}} e^{U/KT}, \quad (2.20)$$

where M is the mass of the NP and R is the molar gas constant.

In the simulations presented here, there is no contribution from an external electric field, as there is no electric field present in the condition under which delivery is carried out in the experiment, but the model can account for an external field by including such contribution in Equation (19).

Elapsed time at each simulation step is then calculated by dividing the mean displacement by the average total velocity for that time step

$$t_n = t_{n-1} + \frac{TMD_n}{\bar{v}_n}, \quad (2.21)$$

where, t_n is the time at step n , t_{n-1} is the time at the previous step $n-1$, TMD_n is the average displacement of all particles during timestep n , obtained as the square root of the Mean Squared Displacement, and \bar{v}_n is the total velocity, from Eq. (2.20), at that time.

2.5 Modelling Pores/ Endcaps at Tube ends

In HNTs purely non-Knudsen transport (because the radius of the nanotube is around 15 nm) at atmospheric pressure and temperature is observed. Here, we present a rather unique 3-D coarse grain Monte Carlo (time –quantified) model that uses classic kinetic theory coupled with Guy-Chapman-Enskog theory and Poisson-Boltzmann theory to describe the molecular transport in the HNT channels with endcaps or pores near the tube's openings. The model, implemented using MATLAB [122], was designed to simulate NP diffusion in long, defect free NTs and out of the ends of the NTs. The hydrodynamic radius, the effective radius of a hydrated NP in the solution, is considered in these simulations, rather than the actual gas phase radius. NPs are considered to be spherical in shape and are initially distributed uniformly throughout the cylindrical channel except at the tube's ends where the density is larger to account for the experimentally observed initial burst, with the channels immersed in a dielectric medium.

NP's motion is simulated based on a concentration-dependent random walk to sample the configuration space subject to collisions and interactions between the NPs and between the NPs and the HNT walls. The motion of the NPs inside the nanotubes is

based on their interactions with their immediate neighborhood; this includes other particles and the surrounding nanotube walls or the nanotube pores/endcaps. Particles are moved one at a time in an arbitrary direction and an arbitrary length up to an upper limit that depends of the kinematics of the system. The change in energy of the system due to the move is calculated to determine if the move is energetically viable at a given temperature. The move is allowed as long as it is energetically viable and there is no overlap with the walls or with neighboring NPs along the line connecting the initial and final position of the NP. There are two ways to model the endcap/pore. Figure 2.3 presents the two distinct geometries considered for this work.

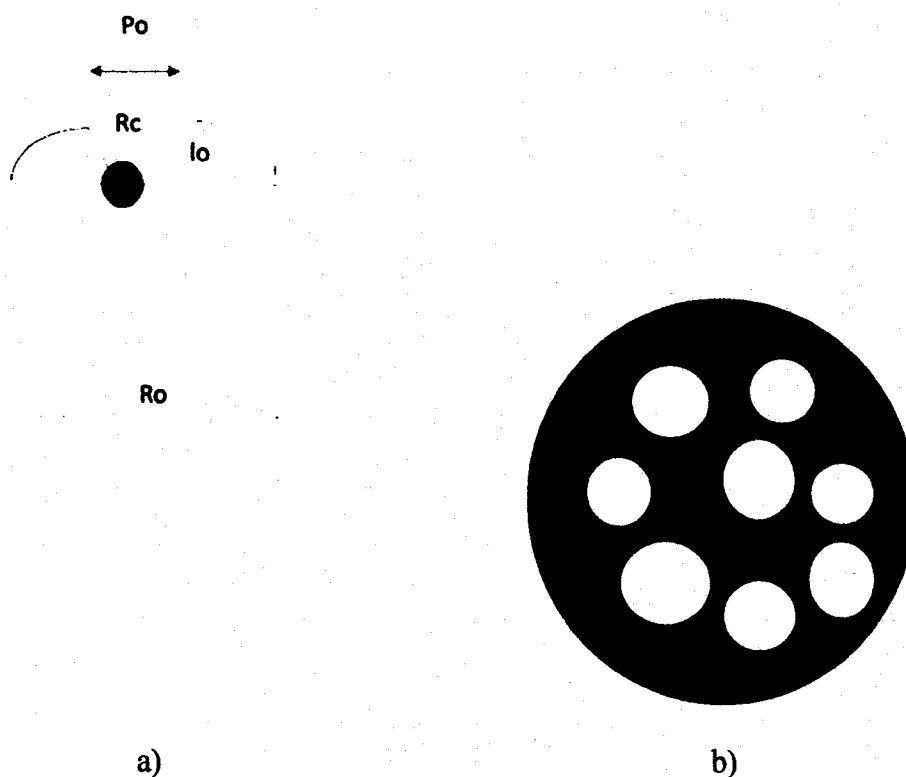


Figure 2.3: a) Single opening pore b) Perforated pore.

At the HNT entrance, the infinity tube approximation is discarded in favor of the interaction between the NP and a rounded HNT pore entrance as schematically

represented in Figure 2.3a. Perforated pores as seen in Figure 2.3b are defined by their total open area which is the ratio of the open area of the disk to the total area of the disk.

2.6 NP- Pore Wall Interaction

The NPs are modeled as soft core spheres with hydrodynamic radius R and a surface potential (the potential at R). The NT's walls are positively charged with a pH-dependent surface charge density. Due to the structure of HNT pores, a soft wall composed of Lennard Jones (LJ) atoms is chosen accordingly. As the NPs approach the pore region at the tube's ends, they experience a Columbic and a VDW interaction with the spherical pore wall. The total energy experienced by the NPs is

$$u(r) = u_{vdw} + u_{CB} \quad Z < 0 \text{ and } Z > L \text{ and } x^2 + y^2 \leq 2R_p, \quad (2.22)$$

where u_{CB} is the energy contributions due to Columbic interactions and u_{vdw} the contributions due to VDW interactions.

The VDW ion-wall interaction can be computed by integrating the VDW potential over the wall's surface. An analytical expression for the VDW experienced by small charges inside a cylindrical nanotube is given by Eq. (2.23).

$$u_{vdw} = \frac{A}{6} \left[\frac{2RR_p}{D^2 + 2(R+R_p)D} + \frac{2RR_p}{D^2 + 4RR_p + 2(R+R_p)D} + \ln \left[1 - \frac{4RR_p}{D^2 + 4RR_p + 2(R+R_p)D} \right] \right], \quad (2.23)$$

where R_p is the radius of the curvature of the pore and D is the distance of separation of the NP from the pore wall, and A is the Hamaker constant and is given by Eq. (2.24).

$$A = \frac{3}{4} kT \left(\frac{\epsilon_w - \epsilon_m}{\epsilon_w + \epsilon_m} \frac{\epsilon_p - \epsilon_m}{\epsilon_p + \epsilon_m} \right) + \frac{3hV_e}{8\sqrt{2}} \frac{(n_w^2 - n_m^2)(n_p^2 - n_m^2)}{\sqrt{(n_w^2 + n_m^2)(n_p^2 + n_m^2)} \sqrt{(n_w^2 + n_m^2) + (n_p^2 + n_m^2)}}, \quad (2.24)$$

where ϵ_w is the permittivity and n_w is the refractive index of the nanotube wall, ϵ_p is the permittivity, and n_p is refractive index of the NPs, and ϵ_m is the permittivity while n_m is the refractive index of the surrounding medium.

The potential energy landscape due to the Columbic interaction between the NP and the inner surface of an endcap/pore is described by Eq. (2.25).

$$u_{CB} = \frac{128\pi R r_p K T n_\infty}{(r+R_p)\kappa^2} \tanh\left(\frac{Ze\psi}{4KT}\right) \tanh\left(\frac{Ze\psi_p}{4KT}\right) \exp(-\kappa D), \quad (2.25)$$

where ψ_p is the surface potential of the endcap, and n_∞ is the bulk density of the ions in the endcap.

When the pore is formed by crosslinking of the HNTs with polymers or by any of the other methods described in the introduction, its shape resembles that of the pore as shown in Figure 1b. For these kinds of pores, the above equations for energy cannot be used. The VDW ion–endcap wall interaction can be computed by integrating the VDW potential over the wall's surface. An analytical expression for the VDW experienced by small charges inside a cylindrical nanotube is given by Eq. (2.26)

$$u_{vdw} = \frac{AR}{6D}. \quad (2.26)$$

The potential energy landscape due to the Columbic interaction between the NP and the inner surface of an end cap/pore is described by Eq. (2.27)

$$u_{CB} = \frac{\epsilon_p \epsilon_0 \psi_p^2 \sinh(\kappa r)}{R^2 r \cosh\left(\kappa\left(R_p - \frac{R}{2}\right)\right)} \quad (2.27)$$

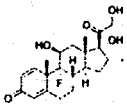
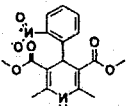
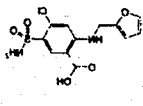
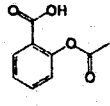
For inert non-polar surfaces the VDW potential energy is given by Eq. (2.28)

$$u_{vdw} = \frac{A}{24\pi D_0^2} \quad (2.28)$$

where D_0 is the cut off distance of separation between the NP from the pore's wall and A is the Hamaker constant.

Time is introduced into the model using the method presented above. We have used dexamethasone for all of these simulations. The relevant physical properties used in our simulations can be found in Table 2.1. The properties of all NPs studied in this work are given in Table 2.1.

Table 2.1: Physical properties of the four different NPs used in this work.

Molecules	$C_{22}H_{29}FO_5$ Dexamethasone	$C_{17}H_{18}N_2O_6$ Nifedipine	$C_{12}H_{11}ClN_2O_5S$ Furosemide	$C_9H_6O_4$ 2-Acetoxy benzoic Acid
ζ (pH 7.5) (mV)	-35	-45	-40	-4
Refractive Index	1.592	1.559	1.658	1.551
Refractivity (cm^3)	102.493	87.9	75.8	44.5
Molar Volume (m^3)	296.2×10^{-6}	272.3×10^{-6}	205.8×10^{-6}	139.6×10^{-6}
Density (g/cm^3)	1.3	1.35	1.6	1.3
Polarisability (cm^3)	39.7×10^{-24}	34.8×10^{-24}	30×10^{-24}	17.7×10^{-24}
Molecular Weight (Da)	392.47	346.33	330.74	180.04
Molecular Radius ($\times 10^{-9}$ m)	0.207	0.198	0.195	0.159
Solubility (mg/mL)	0.1	0.05	0.1	3
Structure				

2.7 Experimental Conditions: Nanotube Loading/Release

All the work reported here is a result of computer simulations; however, in order to give the reader a clear picture of how the simulations represent the experiment, the conditions under which the experiments are conducted are reported here. It is worth mentioning that we have used experimental data and results from Dr. Yuri Lvov's group to validate the simulation.

In order to load the HNT, saturated solutions of drugs is mixed with a dry HNT powder and sonicated for 15 minutes. The samples are transferred into a vacuum jar, which is then evacuated using a vacuum pump. A slight fizzing indicates the removal of air from the HNT lumens. The expelled air is replaced with the saturated solution of drugs. The process is repeated three times for most efficient loading, which is typically 6-8 wt. %. After loading, the samples are separated from the solution by centrifugation, washed and then air dried.

All release experiments are performed in water, at pH 7.5 and room temperature (sink release conditions). The samples are stirred and the supernatants are collected periodically. Concentrations of released drugs are determined using UV-Vis spectrophotometer. At the end of the release study, a high power sonication is performed to ensure the complete release of loaded corrosion inhibitors and to calculate the loading efficiency for the kinetic normalization. More experimental details are given in [113,134,139].

CHAPTER 3

RESULTS AND DISCUSSION

In this chapter we validate the simulation model presented in Chapter 2 using published experimental data. The validated model is used to study the effect of various parameters like HNT's lumen size and length and NP's charge on the release of NPs from HNTs. We discuss in detail the different regions of the release profiles, and the different diffusion mechanisms that govern the motion of the NPs in each of these regions. We use well established mathematical models to obtain the diffusion coefficient in each of these regions.

3.1 Validation of the Model

The results shown in Figures 3.1-3.12 feature the spontaneous release of NPs from HNTs immersed in a medium of constant dielectric properties (water). The term spontaneous release indicates that the NPs motion in the HNT is not driven by externally applied forces or potentials. The diffusion of NPs is driven only by interactions between NPs and HNT and a concentration gradient. Four different NPs, 2-acetoxy benzoic acid, dexamethasone, nifedipine, and furosemide were chosen to validate the model; the experimental release profiles for these molecules from HNTs were obtained from the literature. In the pH range of 4–8.5, surface charge in the HNT tubule lumen is positive and the surface charge on the external surface is negative. This surface charge difference promotes the loading of negatively charged molecules inside the lumen and is expected to

limit their adsorption onto the negative outer surface of the tubules. All the simulations presented here were conducted in an environment consistent with a pH of 7.4 selected to match the experimental conditions to which these simulations are compared to, which replicate physiological conditions for drug release [133].

The release profiles from 12 nm and 15 nm lumen HNTs, in comparison experimental results are shown in Figures 3.1 and 3.2, respectively. Each point is the average of 30 independent simulations under identical conditions.

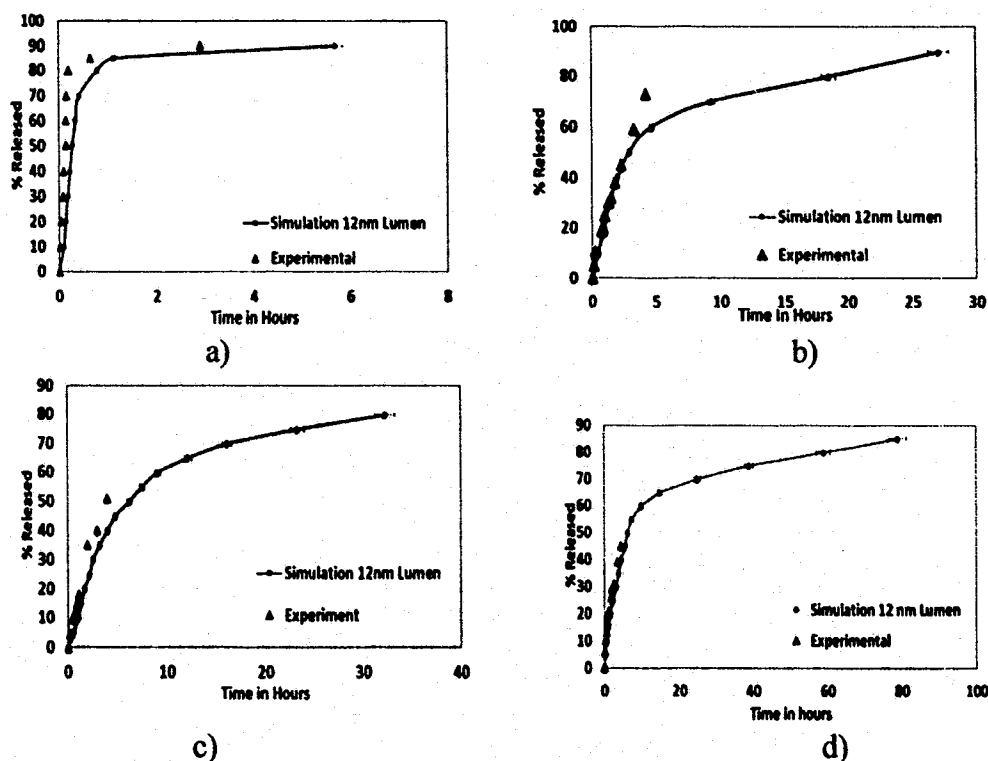


Figure 3.1: Simulation results compared to experimentally available release profiles for a) 2-acetoxy benzoic acid [134] b) dexamethasone [113], c) furosemide [113] and d) nifedipine [113], from a 12 nm lumen HNT.

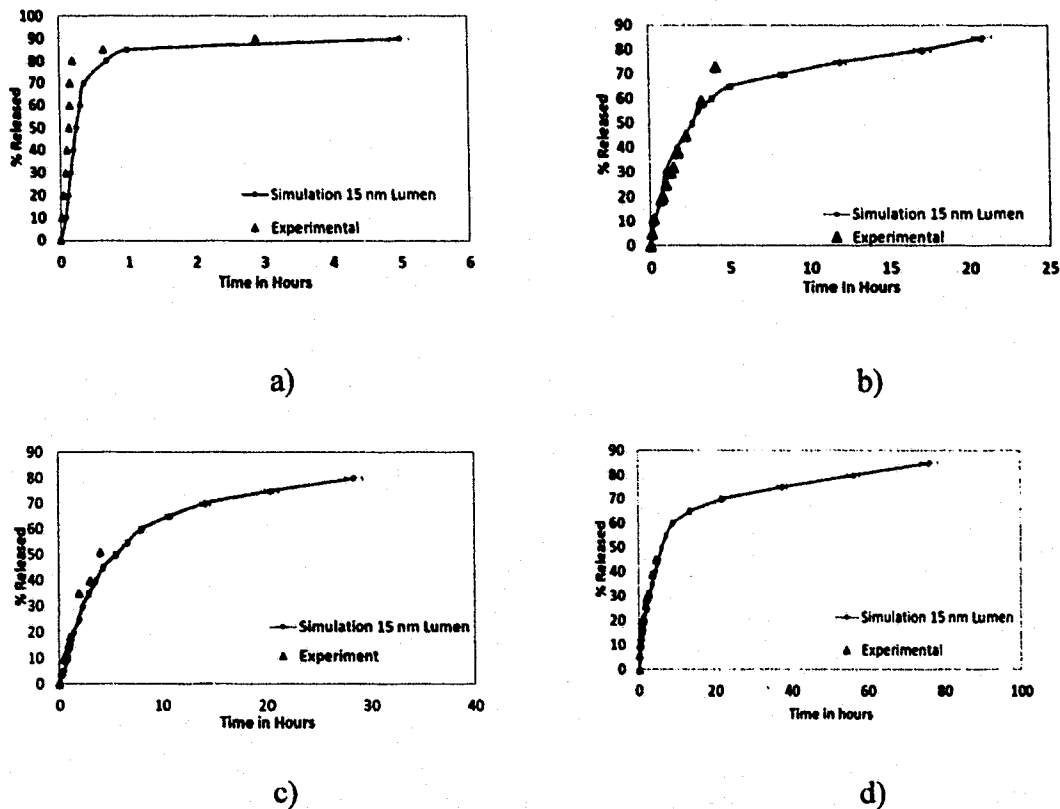


Figure 3.2: Simulation results compared to experimentally available release profiles for a) 2-acetoxy benzoic acid, [134] b) dexamethasone [113], c) furosemide [113] and d) nifedipir [113] d), from a 12 nm lumen HNT.

There is a significant difference between the different batches of HNTs used in the experiments where lumen and length distributions vary from one sample to another, particularly between samples mined from different locations [135-138]. The two lumen diameters selected for the calculations presented above were chosen because the experimental sample for the first three molecules, to which the results are being compared, has a distribution (presented in Figure 3.3) with a peak at 12 nm and average lumen around 15 nm.

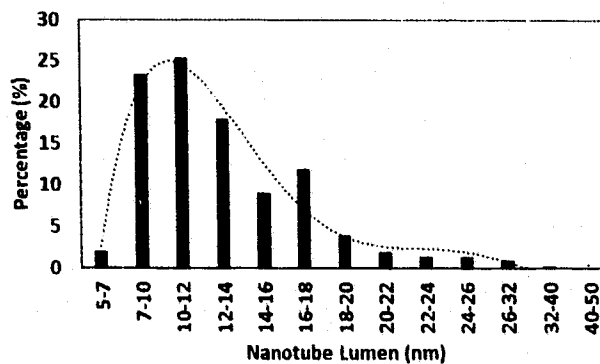


Figure 3.3: Experimentally determined HNT inner lumen diameter distribution [134].

Experiments show that NP release from the Halloysite tubules is typically 25 (nifedipine) – 75 (furosemide and dexamethasone) times longer than that from the micro crystals.³⁶ Table 3.1 shows the time taken for maximum release reported in the experimental work for the four molecules subject of this study. The times reported correspond to 90% release for 2-acetoxy benzoic acid, 70% for dexamethasone, 50% for furosemide, and 45% for nifedipine respectively.

Table 3.1. Comparison of release times from micro-crystals and HNTs [113, 134]

Molecule	Release time from Micro-crystals (Hours)	Release time from HNTs (Hours)
2-Acetoxy benzoic acid [134]	0.05-0.083	3
Dexamethasone [113]	0.16-0.25	14
Furosemide [113]	0.083-0.11	18
Nifedipine [113]	0.25-0.33	6

Figure 3.1a and Figure 3.2a show a comparison between the release profile of 2-acetoxy benzoic acid and experimental results reported by Wenbo Wei [134]. 2-acetoxy benzoic acid has the lowest (negative) zeta potential of the 4 molecules (at pH 7.4), and thus it does not feel as strong a pull towards the walls as the other three molecules leading to the fastest delivery of all. This is clearly shown in Figure 3.1a and Figure 3.2a

where more than 85% of the molecules are released within the first hour. The release profile shows an initial burst followed by a longer saturation phase. The saturation phase is due to the surface diffusion of the molecules adhering to the walls.

Figure 3.1b-d and Figure 3.2b-d provide a comparison between the release profiles for dexamethasone, furosemide, and nifedipine with the experimental release profiles obtained from Veerabadrán *et al.* [113]. These figures show a good correlation between the experimental and simulation profiles. For these cases, simulations also predict an initial burst followed by a saturation face; however, unlike the case of 2-acetoxy benzoic acid, the experimental release stops at a smaller delivery percentage and no experimental verification of the saturation face is provided. These three molecules bear a significantly larger zeta potential than 2-Acetoxy benzoic acid and thus the delivery profile takes longer.

All release profiles have three distinct regions or features. In most release profiles, one of the features is washed out by the other two. These features of the release profile can be explained in terms of molecular interactions. The NPs, being negatively charged, adhere to the HNT's walls and form a layer, similar to a stern layer, near the wall effectively shielding other negatively charged molecules inside the HNT from the HNT wall. These shielded molecules are no longer attracted to the wall, but are driven towards the center of the HNT. Here, they encounter similarly charged NPs. These NPs then diffuse out of the HNT due to intermolecular repulsion. We call this phase the intermediate or axial phase.

These NPs behave like they are in a nanotube made up of like charged NPs with a much smaller lumen. The molecules that stick to the wall diffuse out more slowly,

causing an elongated saturation phase. A large number of NPs aggregated near the HNT openings and in this case the endcap pores diffuse out during the burst phase. Due to this massive diffusion of particles out of the HNTs, the contribution to the total energy of the system due to NP-NP repulsive interactions is greatly reduced, the velocity of the NPs also reduces, and this in turn reduces the NP's release rate in the intermediate phase as time passes. This results in a three-phase release: an initial burst phase or phase I, an intermediate or axial diffusion phase or phase II, and the slower saturation phase or phase III. The presence of phase II is corroborated by the results presented in Figure 4.7 and the release profile of 2-acetoxy benzoic acid in Figure 3.1 and 3.2.

The intermediate/axial diffusion phase is pronounced and prolonged in HNTs with endcaps, as the presence of the endcaps slows down the entire release process. An inspection of the simulation results show that around the concentration where phase III starts, most of the remaining NPs are near the walls. Phase III is therefore governed by surface diffusion along the wall. Phase II is governed by the molecular diffusion of NPs at the center of the tube that are shielded from the wall. In the experiments, phase I is governed by multiple release processes. The first may be attributed to the dissolution of NPs from the HNTs and the endcaps outer openings. The second is the release of NPs in the natural gaps/defects on the cylinder surface at the end of the rolled clay sheet and the NPs accumulated near the pores in the endcaps [139].

In the model, these effects are simulated by setting up a higher NP density at the ends of the tubes than in the center as explained earlier, followed by the release of NPs inside the HNT lumens, shielded from the wall by other NPs. This process is governed by molecular diffusion. The actual concentration at the ends was calibrated *a-priori*, and it is

not used as an adjustable parameter. No single mathematical model can describe the entire release process satisfactorily, but the two phases can be independently described by two distinct mathematical models. Both release phases are concentration-dependent and follows first order kinetics.

The burst phase can be best described by the Korsmeyer-Peppas model [131]

$$\frac{M_t}{M_\infty} = kt^{1-n} \quad (3.1)$$

where M_t/M_∞ is a fraction of the NPs released at time t , k is the release rate constant, and n is the release exponent. The value of n indicates the type of diffusion dominating the process. $0.45 \leq n$ corresponds to a Fickian diffusion mechanism, $0.45 < n < 0.89$ to non-Fickian transport, $n = 0.89$ to Case II (relaxational) transport, and $n > 0.89$ correspond to super case II transport [131]. This is summarized in Table 3.2. The Korsmeyer-Peppas model was first introduced by Korsmeyer *et al.* [131] in 1983 as a simple relationship describing drug release from a polymeric system. This model was used to study the release kinetics of data obtained from *in vitro* drug release studies.

Table 3.2. Interpretation of diffusional release mechanisms from cylindrical channels [131].

Release exponent (n)	Drug transport mechanism
0.5	Fickian diffusion
$0.45 < n < 0.89$	Non-Fickian transport
0.89	Case II transport
Higher than 0.89	Super case II transport

While the Korsmeyer-Peppas Model accurately describes the initial burst phase release, it is claimed to be accurate up to approximately 60% release. A different model

introduced by Weibull and others [132] is better suited to describe the saturation phase release. The Weibull model best describes release profiles and dissolution of drugs from the cylindrical delivery matrixes.

$$\frac{M_t}{M_\infty} = \left[1 - e^{-\frac{t^b}{a}} \right], \quad (3.2)$$

where M_t is a fraction of the NPs released at time t and M_∞ is the total amount of NPs released. Parameter a denotes a scale parameter that describes the time dependence while b describes the shape of the dissolution curve progression. For $b = 1$, the shape of the curve corresponds exactly to the shape of an exponential profile with the release rate constant $k = 1/a$.

The release curves corresponding to a 12 nm lumen HNTs are described below by using the two different mathematical models of first order kinetics discussed above. The results are presented in Figure 3.4 and the fitting parameters are presented in Table 3.3.

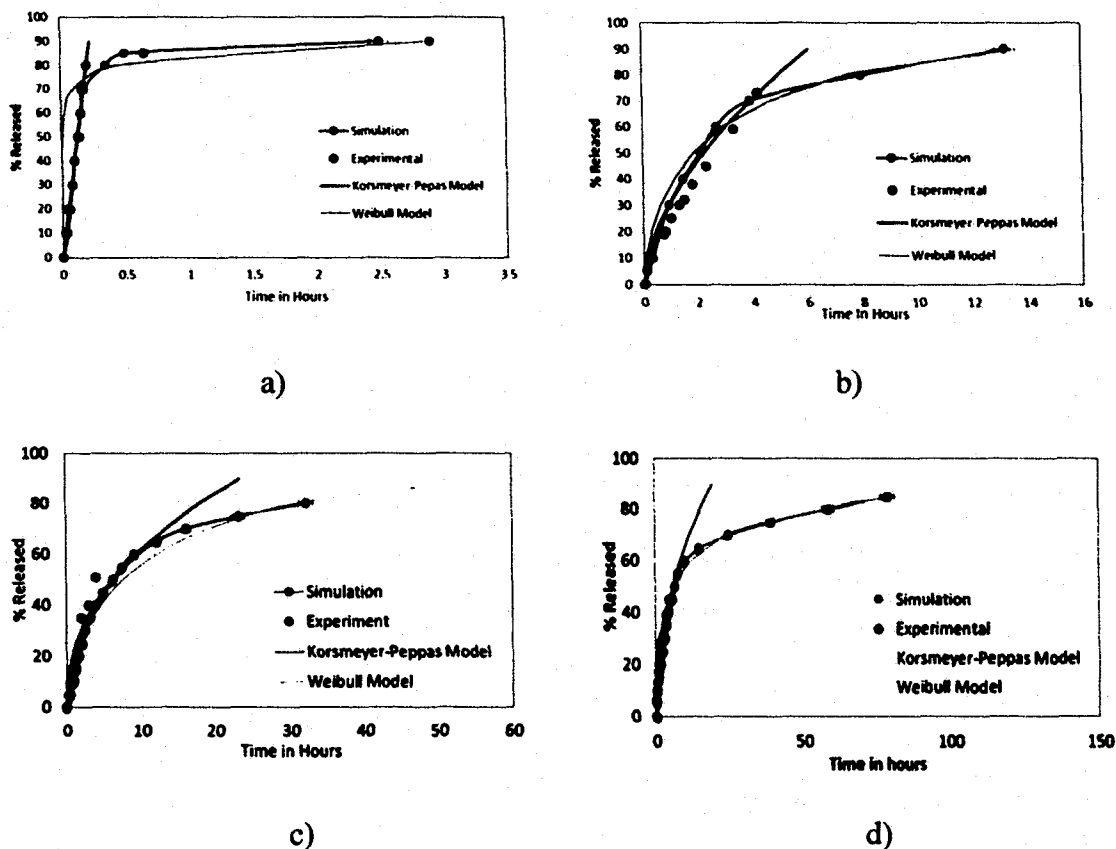


Figure 3.4: Diffusion models compared to simulated release profiles for a) 2-Acetoxy benzoic acid [134] b) dexamethasone [11], c) furosemide [11], d) nifedipine [11].

Table 3.3: Parameters from fitting different models to the release profiles from HNTs. (These parameters are consistent with t in hours)

Molecule	Burst	Phase	Saturation	Phase	$K=1/a$
	k	n	b	a	
12 nm HNTs					
Dexamethasone	0.258	0.42	2.1	0.45	0.47
Furosemide	0.219	0.5519	4.9	0.6	0.2
Nifedipine	0.215	0.519	0.406	3	0.33
2-Acetoxy benzoic Acid	1.915	0.001	0.2	0.6	5

It is observed that as the zeta potential of the NPs becomes more negative (see Table 2.1), the more the release profiles deviate from Fickian diffusion in the initial burst

phase, as evidenced by the values of $n = 0.001$ for 2-acetoxy benzoic acid (the less negative) and 0.55 for furosemide (the most negative).

3.2 Effect of HNT Lumen

As discussed earlier, there is an important variation in HNT and NP properties in the experiment that may affect the release and therefore the effect of each of these parameters on the release profile is studied independently. In this subsection the effect of the inner lumen diameter is addressed. The NP chosen for this study is dexamethasone (see Table 2.1 for this particle's properties). All of the simulations are run at 300 K and the results are presented in Figure 3.5. The HNT lumen varies from 10 nm-50 nm. Error bars are not shown here for clarity, but they are within the same magnitudes as those shown in all other plots.

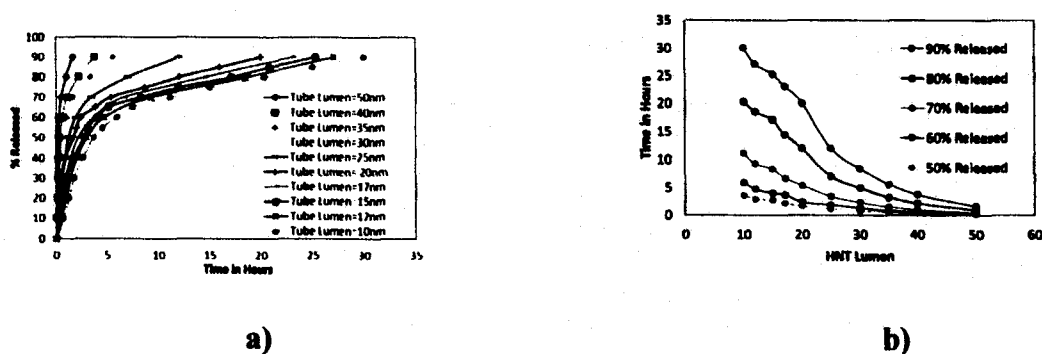


Figure 3. 5: a) Simulated release profiles of dexamethasone molecules from HNTs of different radii. b) Time needed for a given percentage of particles to be released vs lumen diameter.

Experimentally, the HNT length varies from 0.5 to 1.5 μm with an average of 1 μm ; thus, for this study the tube length was selected to be 1 μm . The NPs were placed inside the HNT such that 55-65% of the NPs were placed within the 25% outermost region of the HNT on both sides of the HNT. The diffusion/release profile shows an

increase in the delivery rate with the HNT diameter. In all of these cases, the dexamethasone particles experience surface diffusion at the end of the release, but as the HNT lumen increases, the effect of the walls on particle diffusion is less pronounced and the release profile evolves towards free diffusion. In all cases, the particles that are near the wall are attracted to it shielding the other particles from feeling a similar attraction, but for the smaller HNT, fewer molecules are able to cross a given cross-sectional area at once, thus delaying diffusion.

In addition, for larger HNT a smaller percentage of NPs are near the wall. Thus the saturation phase is reached after a larger percentage of particles are released. Since in the experiment a distribution of HNT lumen size rather than a single HNT size is found, a weighted average following the lumen experimental distribution was considered and the result is presented in Figure 3.6 in comparison with samples with a single lumen size of 12 nm and 15 nm and other distributions of lumen sizes, namely uniform and normal distribution, the latter centered at two different lumen sizes (15 nm and 25 nm). The normal distribution was centered at 25 nm because experimentally HNT have lumens up to 50 nm. Thus, a normal distribution centered at 25 nm is symmetric, while the normal distribution centered at 15 nm was chosen as this is the average experimental lumen size. The results are compared to the experimental release profile obtained from literature. As can be seen, there is a large variation with lumen size distribution. In situations like this, simulations can be of assistance as the data obtained from simulations can be used to predict the release profiles from the different samples of HNT mined at different locations across the globe if the size profile is known.

Results show that although 12 nm and 15 nm lumen tubes are a better fit, the short time portion of the curve, the data obtained when the experimental distribution was used (light blue curve in Figure 3.6) better accounts for the entire 70% release data, showing that the presence of larger tubes is responsible for the larger time section of the curve.

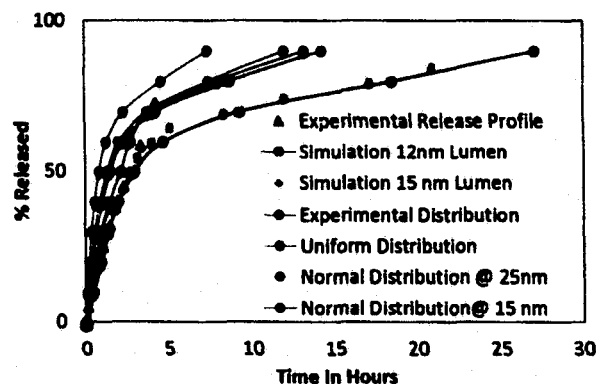


Figure 3.6: Weighted average release profiles of dexamethasone molecules from HNTs of different radii, for various inner lumen diameter distributions.

3.3 Effect of NP Charge

NP's charge undoubtedly has a strong effect in the delivery profile. To address this issue the effect of charge sign (leading to attractive or repulsive interactions) and charge magnitude are studied. Results reported in Figure 3.8 show the variation in release profiles of NPs from HNTs with diameters between 10 nm and 50 nm. The magnitude of the NP's charge is that of dexamethasone (Table 2.1) but with opposite signs. All other properties of the NPs are kept the same (i.e. similar to dexamethasone). The negatively charged NPs experience an attraction towards the nanotube walls, whereas the positively charged NPs experience repulsion. Figure 3.7a shows that for repulsive interactions, the time taken to release decreases with the radius. The particles

experience a squeezing effect and are forced away from the walls towards the center of the nano channel where particle-particle repulsion forces the particles out of the HNT. In Figure 3.7b, the release profiles for attractive interaction from HNT of different radii are shown. The effect in this case is exactly the opposite. The HNT with smaller radii exert a stronger attraction pulling the particles towards them. Once at the wall, the NPs stay there and move along the surface of the wall resulting in surface diffusion. In both cases, the smaller the tube diameter the more pronounced is the effect.

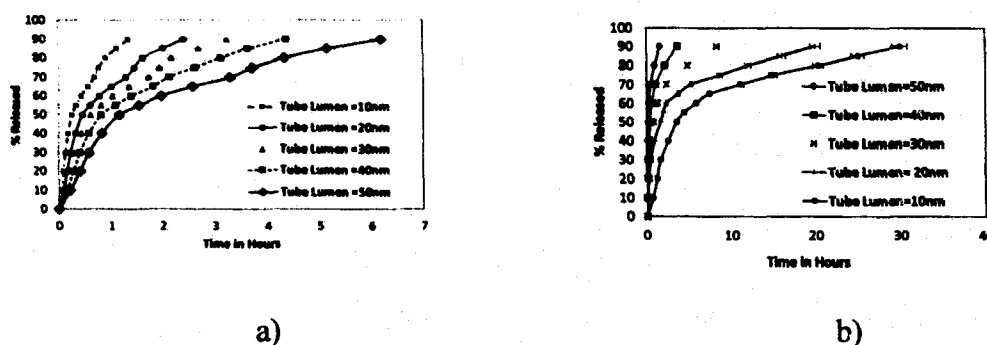


Figure 3.7: a) Release profiles for repulsive interactions between the wall and the particles for different radii. b) Release profiles for attractive interactions between the wall and the particles for different radii.

Next, the magnitude of the NP's charge is considered. All other properties are those of dexamethasone. Changing the net charge of the molecule is experimentally possible by either using layer-by-layer functionalization, or encapsulating the NPs in micelles. All of the simulations are run at 300 K. The NP charge is varied from +3 to -5. The results are shown in Figure 3.8. An increase in the charge on the NP leads to a stronger interaction among the NPs and between the NPs and the charged inner wall of the nanotube. In the case of attractive interactions, the NPs experience a pull towards the wall and the mechanism of diffusion that occurs in all such cases is surface diffusion. As

expected, the particle with the largest charge diffuses more slowly than the less charged particle. In the case of repulsive interactions, NPs experience a push away from the walls and the mechanism of diffusion that occurs in all such cases is normal mode diffusion. Once more, the NPs with the largest charge diffuse faster than the less charged particle. Figure 3.8b shows the time taken for a certain percentage of the particles to be released from the HNT as a function of the charge. For positively charged particles, the release time is very small in the time scale appropriate for negatively charged particles and all points seem to overlap each other making evident the fast diffusion.

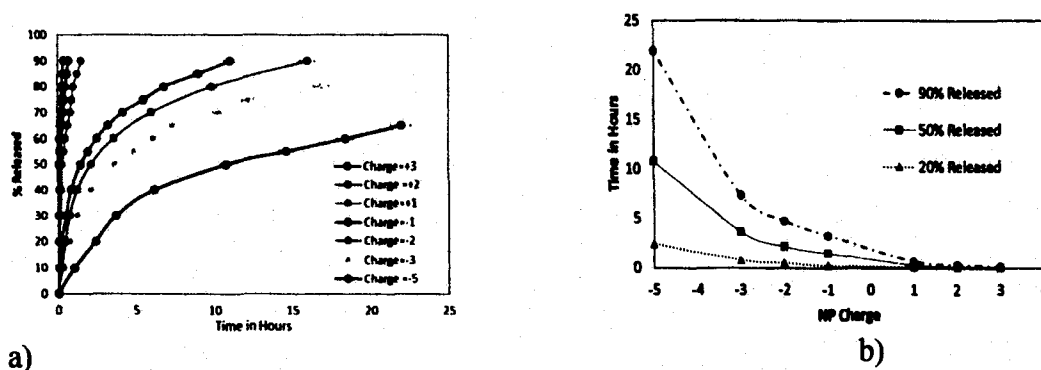


Figure 3.8: a) Release profiles of dexamethasone-like particles with different charges from HNTs of lumen 15 nm. b) Time needed for 20%, 50% and 90% release of NPs Vs NP charge.

3.4 HNT Lumen Corrected Release Profiles

As a corollary of this work, Figure 3.9 shows the release profile of the 4 molecules from a HNT sample weighted for different lumen diameters with a distribution presented in Figure 3.3. A much better agreement with experimental results is observed compared to what is shown in Figure 3.1 and Figure 3.2. Accounting for the experimental distribution of HNTs length, may improve the agreement further.

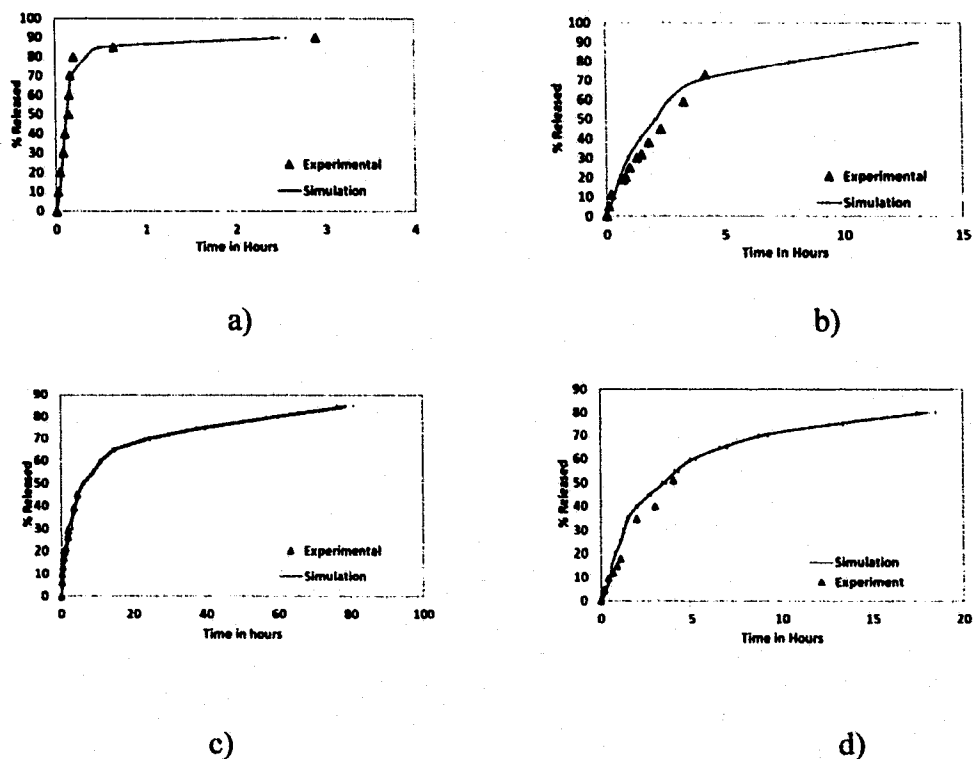


Figure 3.9: Comparing the experimental and weighted average simulated release profiles of a) 2-acetoxy benzoic acid [134] b) dexamethasone [113], c) furosemide [113] and d) nifedipine [113].

3.5 Effect of HNT Length

A disadvantage of HNTs is that the lumen volume is only 10-14% of the total volume so loading efficiency is limited. To increase loading, the lumen properties such as lumen volume, internal charge, etc. can be tuned. Lumen volume is determined by two parameters: the lumen diameter and HNT length. Figure 3.10 shows the effect of tube length on the release profile of dexamethasone NPs from 15 nm lumen HNTs at 300 k. The initial concentration density in all tubes is the same. As can be seen, the release is slower for longer HNT; however, notice that in all the cases, the saturation phase starts at about the same concentration. In this case after 60% of the particles have been released.

This clearly contrasts with the effect of lumen radius where the saturation phase starts after a larger percentage of particles has been released for larger HNT. The larger HNTs release the NPs faster. There is a direct correlation between the length of the tubes and the rate of release of NPs.

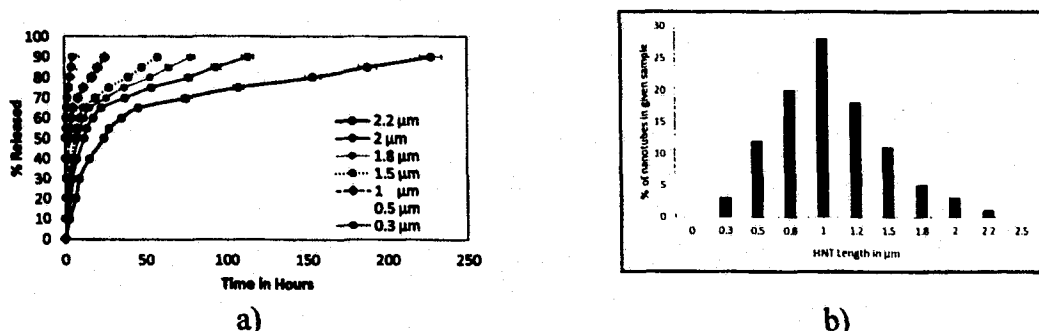
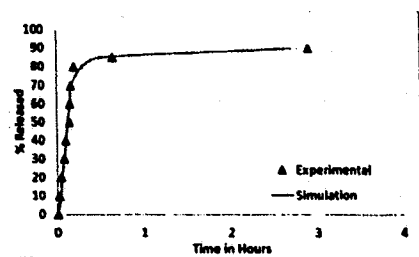


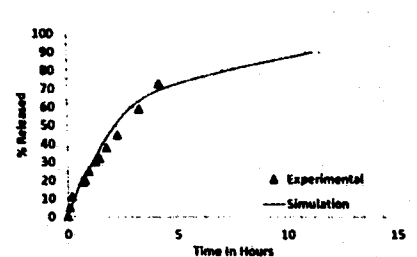
Figure 3.10: a) Simulated release profiles of dexamethasone molecules as a function of tube length b) Length distribution of a sample of HNT.

3.6 HNT Lumen and Length Corrected Release Profiles

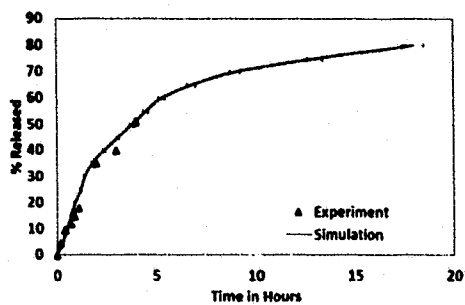
As a corollary of this work, Figure 3.11 shows the release profile of the four molecules from a HNT sample weighted for different lumen diameters and lumen lengths with distributions presented in Figures 3.3 and 5.4b, respectively. A much better agreement with experimental results is observed compared to what is shown in Figure 3.11. Accounting for the experimental distribution of HNT length clearly improves the agreement between experimental data and simulation results.



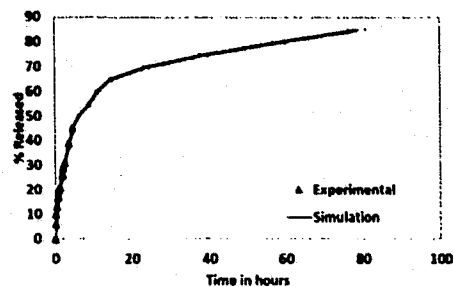
a)



b)



c)



d)

Figure 3.11: Comparing the experimental and weighted average simulated release profiles of a) 2-acetoxy benzoic acid [134] b) dexamethasone [113], c) furosemide [113] and d) nifedipine [113].

CHAPTER 4

SUSTAINED RELEASE FROM HNTS WITH ENDCAPS

In the previous chapter, we validated the simulation model and studied the effect of various parameters like HNT lumen size and length and NP charge on the release of NPs from HNTs. In this chapter, the modification of the release profile by static blocking with inert endcaps to obtain long-term release of NPs from HNTs is studied. Endcaps help ensure the NPs inside the HNTs are released in a much more prolonged and sustained manner, with release times of hundreds of hours. Two basic endcap geometries, spherical and planar, have been considered for this study. Single pore and multi pore are considered for the case of planar endcaps 2 configurations.

4.1 HNTs with Spherical Endcaps

Figure 4.1 contains a schematic of the typical formation of endcaps at HNT ends.

One of the more commonly used endcap material is silica.

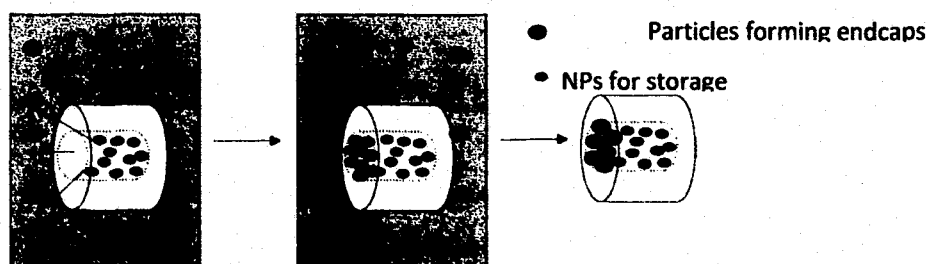


Figure 4.1: Schematic depicting typical end cap formation.

Results shown in Figure 4.2 feature the spontaneous release of NPs from HNTs with end caps, immersed in a medium of constant dielectric properties consistent with water. The term spontaneous release indicates that the NPs motion in the HNT is not driven by any externally applied forces or potentials, but driven only by interactions among NPs and between NPs the HNTs' walls and endcaps, and a concentration gradient. In the pH range of 4–8.5, surface charge in the HNT tubule lumen is positive and surface charge on the external surface is negative. This surface charge difference promotes the loading of negatively charged molecules inside the lumen and is expected to limit their adsorption onto the negative outer surface of the tubules. All the simulations presented here were conducted considering a pH of 7.4 which replicate physiological conditions for drug release. The HNT's lumen was 12 nm in diameter [26].

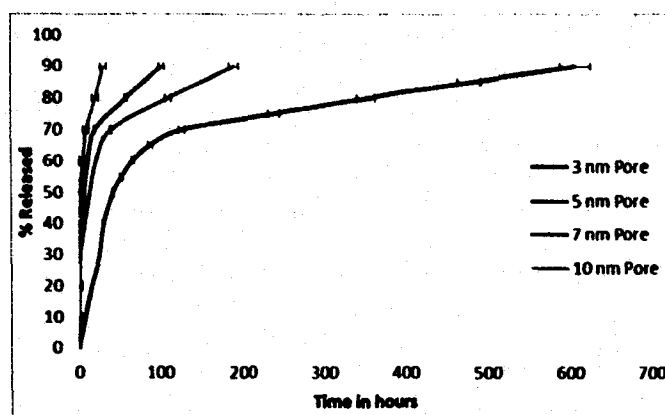


Figure 4.2: Release profiles of dexamethasone Molecules from HNTs with neutral spherical endcaps with a single pore of different pore's radii.

Considering an attractive interaction between the particles and the wall (as is the case), and with neutral or uncharged porous endcaps, the particles experience a pull towards the HNT walls. Figure 4.3 shows how the release profiles of dexamethasone changes as a function of the endcap pore radius; as it can be seen, the smaller the endcap

radii the slower is the out diffusion of particles. The effect in this case is due to the smaller opening at the tube's ends. These smaller openings lead to a decreased diffusivity and a slower release of the drug from the nanotube. The NPs naturally accumulate near the tube's openings and as the concentration of NPs near the tube's endcaps increases, the other NPs inside the nanotube are repelled from the openings. At the same time NPs near the pore opening are pushed out by the particles in the main part of the HNT. The intermolecular repulsion is then what drives out most of the NPs near the tube's opening.

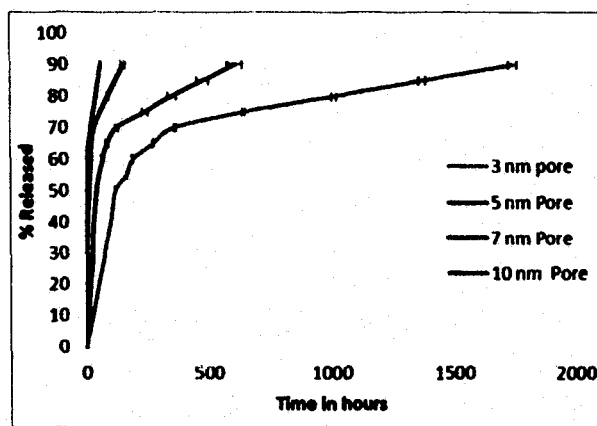


Figure 4.3: Release profiles of dexamethasone Molecules from HNTs with charged spherical endcaps for different single pore with different radii.

In the case of charged endcaps, with charges that are similar to that of the HNT's wall, the effect of the pore on the release profile is even more pronounced (Figure 4.5). The NPs are attracted to the wall and stick to it. A very slow surface diffusion along the pore's walls is responsible for NP's release. This results in a marked increase in release times enabling a more sustained and controlled release of the drug from the nanotubes. As in the previous case, a smaller pore's radius leads to a much slower release of NPs from the HNT that is now further delayed by the repulsion caused by the caps extending the release to thousands of hours.

4.2 HNTs with Planar Endcaps

Figure 4.4 shows the release profile from HNT comparing flat with spherical caps with a single 3 nm pore in both cases. The release from the HNT with the flat disk pore is slower than for the spherical pore because the spherical pore allows charges to accumulate near the pore with the cap acting like a funnel; therefore, more NPs are able to get closer to the pore's opening and are pushed out of the pore due to the dominating NP-NP repulsion.

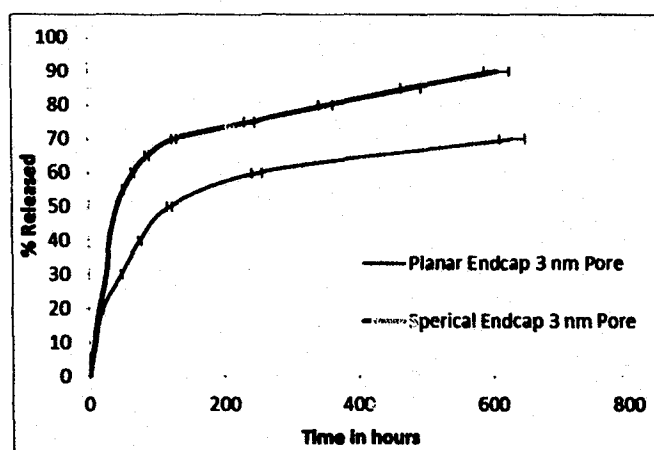


Figure 4.4: Release profiles of dexamethasone Molecules from HNTs with spherical endcaps and flat endcaps with pore of diameter 3 nm.

For planar endcaps, with several as opposed to one pore, the rate of diffusion depends on the number of pores in the endcaps and the radius of those pores. To study the dependence of the release profile with these parameters, release profile is calculated as a function of a factor A that determines the percentage of the cap that is open through which the NPs diffuse out,

$$A = \frac{\text{Total area of all the holes}}{\text{Total area of the disk}} * 100. \quad (4.1)$$

A is varied by first varying the number of pores while keeping their area constant and then by varying the area of these pores but maintaining their fixed number. All of the pores, however, have sizes larger than the diameter of the NPs.

In Figure 4.5a, A varies by increasing the number of pores but keeping the area of these pores equal to 1 nm, while in Figure 4.5b, A varies by changing the pore size, but the number of pores is constant (two).

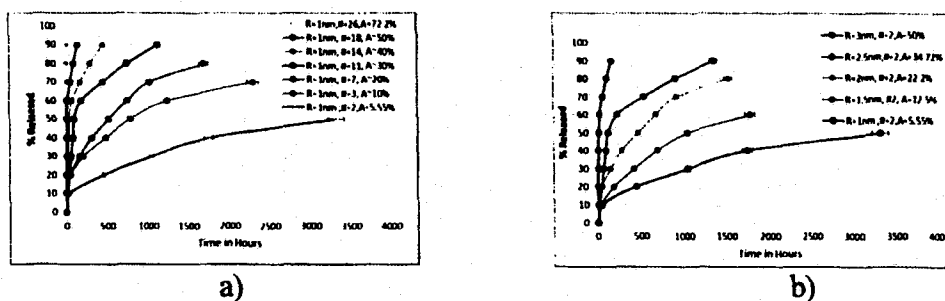


Figure 4.5: a) Release profiles of dexamethasone molecules from HNTs with perforated endcaps for different values of A by changing the number of pores by keeping the radius to 1 nm b) Release profiles of dexamethasone molecules from HNTs with perforated endcaps with fixed number of pores (2) but different radii.

As expected, release time decreases with an increasing value of A . In the first case, the larger number of pores allow for more NPs to be released simultaneously. Increasing the pore size seems to produce a similar effect as curves look rather similar. In order to establish the relative importance of pore size vs. number of pores, two different caps with nearly the same value of A ($A \sim 50\%$) are studied. Figure 4.6 shows the release profiles of both these cases. The results show a significant overlap of the release profiles. Factor A seems to be a significant parameter. However, with smaller pores, release occurs faster than with less but larger pores. This could be explained by the reduced competition (NP-NP repulsion) as they go through the pores, larger pores allow more particles to go

through but they will be closer to each other than if they go simultaneously through different pores. The simulations are stopped when 90% of all NPs are released or when there is no significant change in number of particles released for 100 hours.

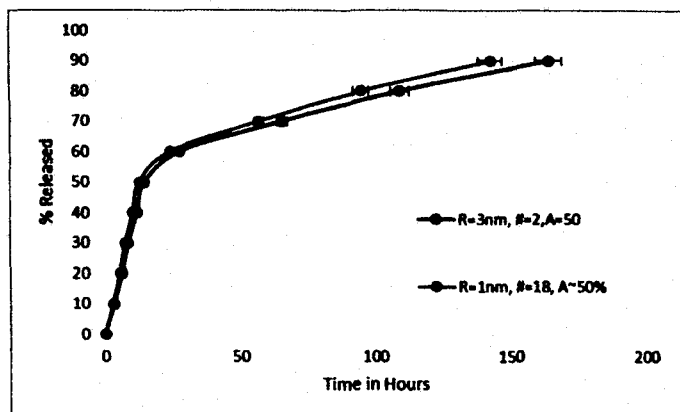


Figure 4.6: Simulated release profiles of dexamethasone NPs for two distinct configurations of planar endcaps.

4.3 Charged Endcaps

The effect of the charge on the caps is also studied here. Planar endcaps are considered; with a charge similar to the HNT walls, an attractive interaction between the NPs and the endcap walls develops.

All release profiles have three distinct regions or features. In most release profiles, one of the features is washed out by the other two. In the release profiles shown in Figures 4.7a and b, it is observed that for smaller values of A , the presence of the three phases in the release discussed in Chapter 3 are more evident, particularly in phase II where it shows up more clearly than in other cases.

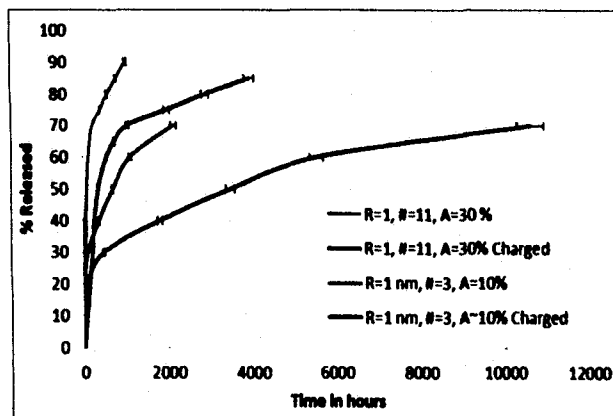


Figure 4.7: Release profiles of dexamethasone from 2 different perforated pore openings for both charged and uncharged pores.

The intermediate/axial diffusion phase is pronounced and prolonged in HNTs with endcaps, as the presence of the endcaps slows down the entire release process and accentuates each phase.

Simulations show that NP release from the HNTs with endcaps is typically 200-400 (dexamethasone) times longer than that from the micro crystals and 25-75 times longer for HNTs without endcaps.

CHAPTER 5

DELIVERY DUE TO EXTERNAL STIMULI

In the previous chapter we studied the further delay in the release profiles realized by static blocking with inert endcaps which provides limited control on release profile. To obtain long-term release, as well as on demand delivery, however, new mechanisms that provide sustained delivery and controllability are desired. The introduction of stimuli-sensitive materials into delivery systems improves their controllability and is helpful to realize on-demand release [141-147]. HNTs are well suited for use as stimuli-responsive controlled release systems. HNTs respond to several external stimuli, including pH and temperature. These stimuli have been proposed as triggers for releasing the NPs from the HNT lumens on demand. To obtain extended release times, but particularly on demand controlled delivery, the effect of various control parameters, such as pH and temperature, need to be studied.

5.1 Effect of HNT Length

In the previous chapters, it was shown that the simulated release profiles for NPs from a HNT sample show a better agreement when calculations are weighted for different lumen diameters with an experimentally obtained distribution. This was the case for all four NPs studied in that work. However, in naturally occurring HNT samples, along with lumen size, the HNT length also varies. In Figure 5.1 a), a TEM image of HNT batch, the

diversity in the HNT lumen size can be appreciated, while in Figure 5.1b), the SEM image shows the diversity in the HNT length for a similar sample.

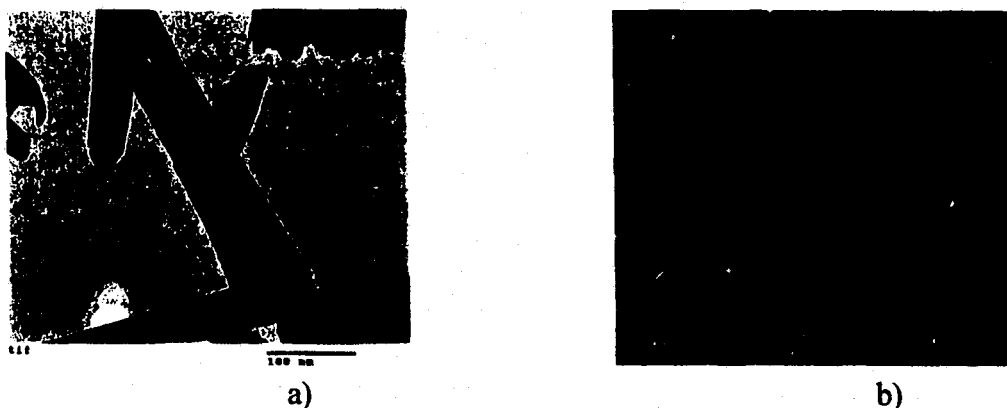


Figure 5.1: a) TEM images of HNTs showing diversity in HNTs Lumen distribution. b) SEM images showing the diversity in HNT size.

Figure 5.2 shows the effect of tube's length on the release profile of dexamethasone NPs from 15 nm lumen HNTs at 300 k. Figure 5.2b shows the experimentally determined HNT length's distribution [134]. The initial concentration in all tubes is the same. As can be seen, the release is slower for longer HNTs, with the saturation phase starting at about the same concentration: in this case, after 60% of the particles have been released. This contrasts with the effect of the lumen radius where the saturation phase starts after a larger percentage of particles have been released for HNT of a larger diameter.

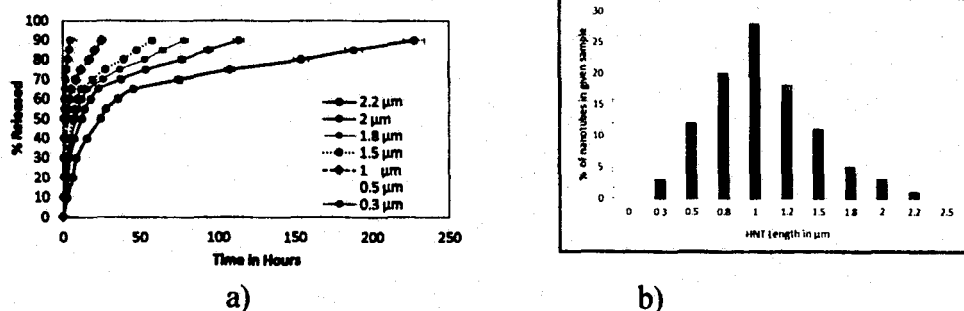


Figure 5.2: a) Simulated release profile of dexamethasone molecules as a function of tube length b) Experimentally determined HNT sample length distribution.

Figure 5.3 shows the release profile of the dexamethosone molecules from different HNT samples. The first release profile is from 1 μm long 12 nm lumen HNTs; the second release profile is from 1 μm long 15nm lumen HNTs; the third release profile is weighted for different lumen diameters (as in Chapter 3); and the fourth release profile is weighted for different HNT diameters, with a distribution of diameters as reported elsewhere [44] and for different lengths, with a distribution presented in Figure 5.1b. Table 5.1 shows the mean squared deviation obtained for HNTs with different lumen and length distributions when compared to the experimental release profiles. Figure 5.3 shows the release profiles compared to the experimental data. Simply considering a distribution of HNT lumen improves the release profile by decreasing the error more than 15 times compared to the release profile from 15 nm lumen HNT, which is the case that provides the best agreement with the experiment when only a single radius and length are considered. When a distribution of lengths is also incorporated in the average, the deviation decreased another 5 times, about 2 orders of magnitude compared to a uniform HNT size distribution.

Table 5.1: Mean square deviation from the experimental prediction of the release profile for dexamethasone. For the first three cases, all HNTs are of a 1 μm in length.

%Released	12nm Diameter	15nm Diameter	Average (Lumen Distribution)	Average (Lumen and Length Distribution)
10	0.065	0.006	0.012	0.0023
20	0.014	0.009	0.048	0.010
30	0.004	0.096	0.133	0.027
40	0.022	0.017	0.163	0.033
50	0.067	0.0004	0.345	0.069
60	1.903	0.417	0.384	0.077
70	26.953	18.046	0.037	0.0078
Average Error	4.147	2.656	0.160	0.032

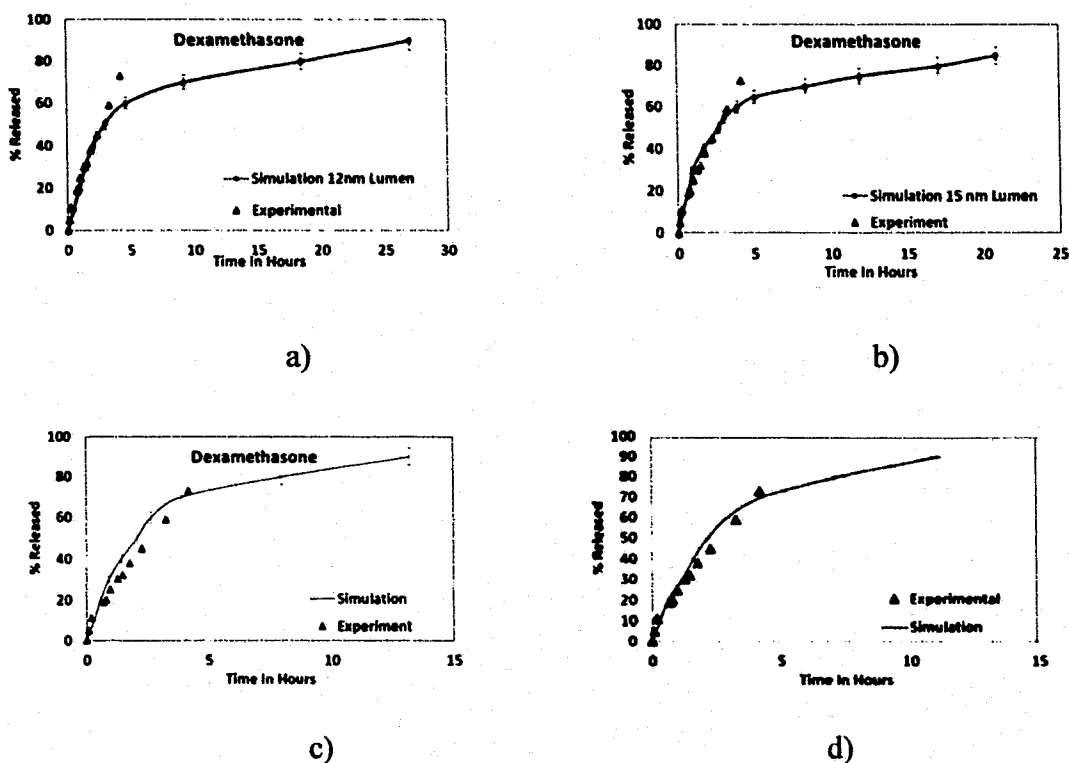


Figure 5.3: Experimental vs simulated release profiles for dexamethasone a) from 1 μm long 12 nm lumen HNTs. b) from 1 μm long 15 nm lumen HNTs, c) from 1 μm long HNTs and release profile weighted for different lumen diameters and d) release profile weighted for different lumen diameters and lumen lengths.

5.2 Three Phase Release

NP-NP and the NP-surface interactions determine the release rate of NPs from the HNT. Two phases experimentally identified in the release profile, namely the initial burst phase, governed by molecular diffusion, and the saturation phase, which is mostly surface diffusion, have been previously characterized and explained in Chapters 3 and 4.

However, when the particle-wall interaction is attractive, an intermediate axial diffusion phase is predicted which has been overlooked to this date. At a given concentration, enough particles will already be near the walls to shield the others from the wall. The

particles in the HNT that are not near the wall are then near the axis of the HNT, shielded from wall attraction, and will diffuse faster due to intermolecular repulsion. This is illustrated in Figure 5.4 which shows the release profile of dexamethasone from a HNT at a pH of 12. It is important to note that when NP-wall interaction is attractive, all release profiles in general have the three regions described here; however, in many cases the intermediate axial regime overlaps with the other two phases, particularly the burst phase, and it is not easily discernable.

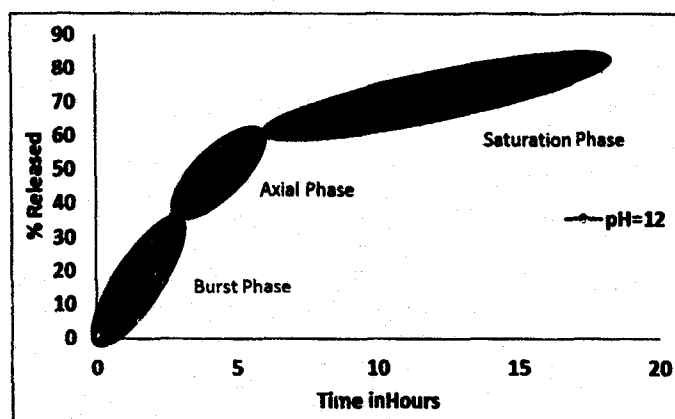


Figure 5.4: Release profile of Dexamethasone-like particles highlighting the 3 different phases.

5.3 Effect of Ambient Temperature

Because temperature stimulus can be easily designed and controlled, it is important to understand the thermal response of HNT delivery systems; therefore, the effect of temperature on the release profile is studied. The temperature in some systems can only be varied by a few degrees, especially for application such as drug delivery, so in the first part of this study changes of ± 10 K from 300 K were studied. In these simulations only the temperature is varied, all other parameters, like HNT surface charge density (consistent to that at pH 7.4) or HNT lumen diameter and length, are maintained

constant. The NP used in these simulations is dexamethasone. Figure 5.5 shows the effect of temperature on the release rate. An increase in temperature increases the total energy of the system and the thermal velocity of the particles. From the point of view of the simulation, the increase in temperature allows some of the rejected hops to become energetically viable/accepted, which in turn results in an increased net displacement of the molecules reducing the transit time. Two competing effects come into play, NPs can go farther faster due to thermal stimuli, but they are still constrained by the geometry of the nano channel and the presence of the surrounding media. From Figure 5.5b it can be seen that a change temperature by ± 10 K has no significant effect on the release profile. This indicates that the increase in temperature by these trivial amounts is expected to produce a negligible effect in the experimental profile.

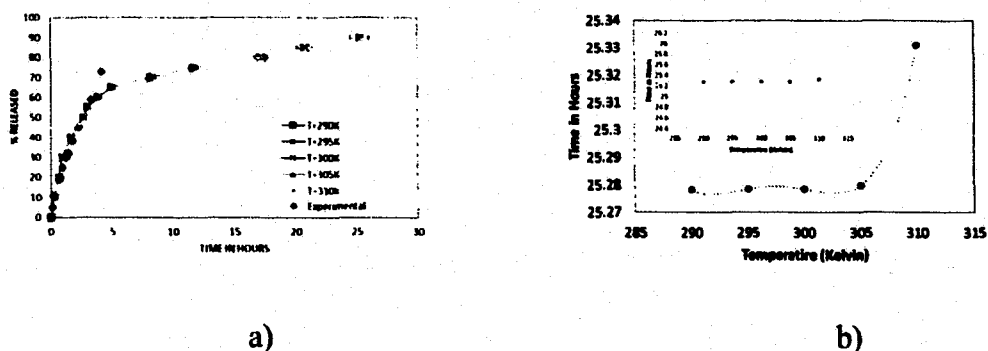


Figure 5.5: a) Release profile for dexamethasone from 15 nm lumen HNTs as a function of temperature. b) Time needed for 90% release of NPs vs Temperature. The inset shows the same information but at a scale needed to accommodate the simulation error showing that all points are indeed within the statistical error.

Temperature is either set by the delivery conditions (like in physiological systems) or it could be controlled to optimize the process. Temperature in some systems can only be varied by a few degrees. For application such as drug delivery, in Figure 5.5

the effect on the release profile of changes in temperature of ± 10 K around 300 K was studied and it was observed that the effect on delivery is negligible. It is expected then that temperature will not be a factor for delivery in live physiological tissues. However, larger changes in temperature may happen or may be desirable for other application, for instance temperatures in the range of 350-400 Kelvin is justified when HNT loaded with antioxidant molecules is used for antiaging doping of rubber tires [52] or antimicrobial geo-polymer concrete, for example [140]; thus, the study is extended to temperatures from 200 K to 600 K. Results are shown in Figure 5.6. Release profiles are clearly different at different temperatures, particularly, above room temperature (400 K- 600 K), the release speeds up by several hours, from 20 hours at 300K, to less than 10 hours at 400 K to less than 1 hour at 600 K. Thus, if release is expected to be controlled at such high temperatures, other mechanisms may be necessary to extend release times. Consistent with this is the observation that at 200 K, the release increases by a factor of about 3 over the release at room temperature.

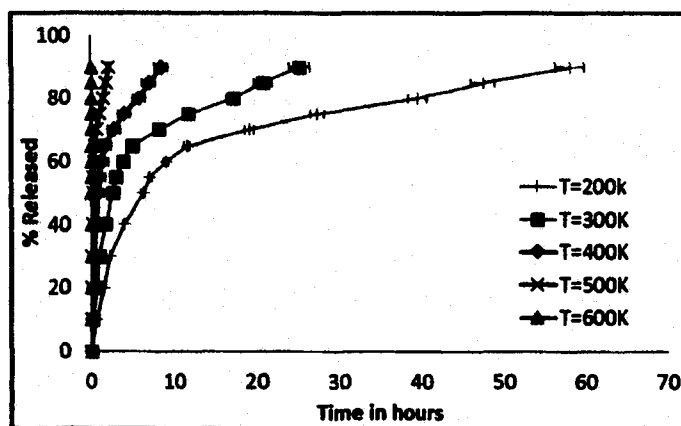


Figure 5.6: Release profiles for dexamethasone from a 15 nm lumen 1 μ m long HNTs as a function of temperature.

5.4 Effect of Surface Potential and pH

Negatively charged NPs experience an attraction towards the walls, whereas positively charged NPs experience repulsion. For a given HNT inner surface charge, the magnitude of the NP's charge determines the strength of the interaction among NPs and between NPs and the HNT walls. When in a dielectric media, the zeta potential (z) is however a more appropriate way to characterize interactions. Z is the difference in electrostatic potential between the surrounding media and the stationary fluid layer attached to the particle, and it depends on the surface charge density, the dielectric media, and the pH. The relation between these values is captured through the Grahame equation [148]

$$\sigma_d = \sqrt{8kT\epsilon\epsilon_0 n} \sinh\left(\frac{zei}{2kT}\right), \quad (5.1)$$

where σ_d is the surface charge density, i is the charge of the protons in the solution, z is the zeta potential, and n is the ionic density in the surrounding solution. Changing the surface charge of the molecule, the zeta potential is experimentally possible by either using layer-by-layer functionalization, or encapsulating the NPs in micelles.

In this study, z is varied from -10 to -55 (the zeta potential of dexamethasone is -35mV in water at pH 7.4) and the results are shown in Figure 5.7. An increase in the NP's surface potential leads to a stronger repulsion among NPs and a stronger interaction between the NPs and the charged HNT inner wall. In the case of attractive interactions, as is the case for dexamethasone, the NPs experience a pull towards the wall, and as expected, the particles with the largest surface potential diffuse more slowly than the ones

with the smaller surface potential. Figure 5.7 shows the release profile until 90% of particles are released for different values of the zeta potential.

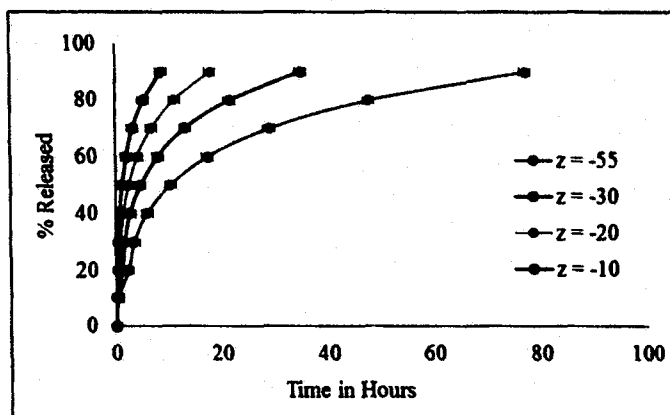


Figure 5.7: Release profiles of dexamethasone-like particles with zeta potentials from HNTs of lumen 12 nm.

Another reason the zeta potential can change is the pH; however, the surface potential of both the HNTs wall and NPs changes with a change in pH as opposed to just a change in the z of the particle as considered in the previous case. In Figure 5.8 the results are presented to capture the effect of pH. Four different values for the pH, namely 1, 6.8, 7.4 (neutral), and 12 were tested to sample pH from acidic to basic.

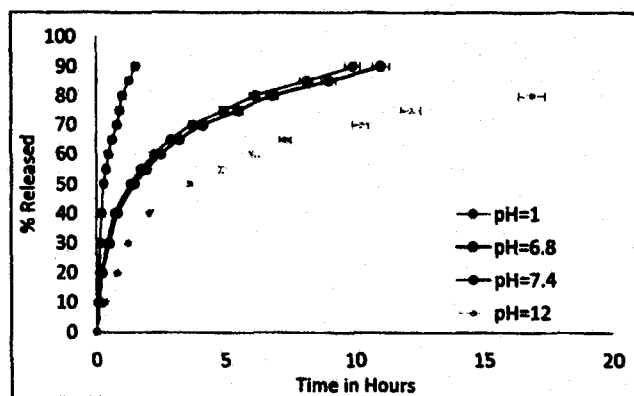


Figure 5.8: Release of dexamethasone like particles for different pH.

At pH 1, the media is acidic, and both the HNT surface and the NPs become protonated, and thus more positively charged. Dexamethasone NPs, which have negative values of z at a pH of 7.4 bare a positive z at lower pH, and the interaction potential with the wall becomes repulsive; NPs are forced away from the walls and inter particle repulsion dominates by propelling them outwards. At pH 12, the HNT lumen is still positively charged and the surface potentials of the NPs are more negative than at 7.4. They then experience a stronger attraction to the HNT-lumen walls.

Among the two stimuli studied, pH-responsive HNT systems are more suitable for use as drug delivery vehicles to cancer cells and inflamed tissues. For instance, it is known that the environment in cancer cells is more acidic than in the blood and normal tissues; thus, the zeta potential in the HNT's inner wall of the HNT and that of the NPs can be adjusted by functionalization so that at neutral pH (7.4) the interaction is attractive, while in the acidic media of a cancer cell, both of them become positive for immediate release. Such systems can also be used to treat clinical disorders like diabetes as the pH of blood changes with sugar content. Certainly, more research (particularly experimental research) need to be conducted to determine the limitations in the ability to control the release and clinical studies conducted to confirm this behavior; however, these simulations show that some control in the trigger mechanism and delivery rate is possible.

The model was used to simulate the diffusion/release profiles of NPs from rigid, defect-free HNTs to study the effect of temperature, zeta potential, and pH on the release of dexamethasone NPs from rigid cylindrical HNTs. When the particle-wall interaction is attractive, an intermediate phase between the already known and characterized burst

phase and saturation phase, that has been hinted in our previous work, but overlooked in the literature to this date, is verified and further explained here. Particles near the walls shield the others and diffusion is now dominated by NP-NP repulsion near the HNT axis.

In terms of release controlled by environmental conditions, the effect of temperature on the release was studied in the large range of temperatures from 200 K to 600 K, relevant to delivery of anticorrosive and antiaging agents in materials (particularly the high temperature end) and demonstrate a significant effect, unlike what was previously predicted for physiological systems, where NP delivery is shown insensitive to temperature due to the much smaller range of temperatures relevant to those processes. To control particle delivery at high temperatures (100 K above room temperature or more), other mechanisms may be necessary. Finally, it is found that in acidic environments, the release of dexamethasone and like molecules is faster when compared to the release profile at pH around 7.4, as the NPs become positive and repulsed from the wall. At higher pH (basic condition), however, a much more sustained release is observed. These results show that the pH of the surrounding media can be used as a control parameter to vary the rate of diffusion of molecular species from multi-walled nanotubes.

CHAPTER 6

CONCLUSIONS

A model to simulate the diffusion/release profiles of NPs from rigid, defect-free HNTs is presented; 2-acetoxy benzoic acid, dexamethasone, nifedipine, and furosemide are chosen as case studies to help validate the model, which in turn has helped identify, at a microscopic level, the relevant interactions controlling the release process and their relative importance in the release outcome. Complete release of non-encapsulated microcrystal dexamethasone is experimentally observed to occur within 10-15 minutes, while a 70% release of this drug takes 14 hours when released from HNTs. Similar behavior can be observed for the other NPs studied (Refer Table 2.1).

The NP-NP and the NP-surface interactions determine the rate of release of NPs from the HNT. Two phases, experimentally identified in the release profile, namely the initial burst phase and the saturation phase, has been characterized and explained. The first one is governed by molecular diffusion and can be best described by the Korsmeyer-Peppas model. The saturation phase is mostly surface diffusion and is mathematically described by the Weibull model. However, an intermediate phase was predicted that has been overlooked to this date. When the particle-wall interaction is attractive, at a given concentration, enough particles will already be near the walls to shield the others from the wall. These shielded NPs will diffuse faster due to intermolecular repulsion as well as the repulsion they experience from the molecules on the wall.

It is found that tunable controlled release can be achieved by varying the HNT lumen diameter and length. Increase in lumen radius leads to a progressive evolution towards free diffusion shifting the saturation phase that occurs after a larger percentage of particles has been release for wider HNTs. Changes in HNT's length also change the release speed, but the beginning of the saturation phase is not affected. Key results show that the diversity of HNT sizes in experimental samples is a main factor in explaining experimental profiles; particularly, a better agreement between simulation and experiment is observed when a similar distribution of HNT lumen diameter and length are considered in the simulation. Other factors affecting the release rate from HNTs such as ambient temperature, pH, and particle charge and zeta potential of the particle were analyzed in detail to determine their effect.

The release rate depends on the NP's charge. Positively charged NPs are released much faster due to repulsive interactions with the lumen walls which are positively charged at pH 7.4: the larger the charge the faster the release. Negatively charged NPs see the opposite effect: the larger the charge the longer it takes for the NPs to be released. Both cases i.e. attractive and repulsive interactions show a radius-dependent diffusion. Varying the ambient temperature by ± 10 K from 300 K does not lead to an appreciable change in the release profile, whereas doubling the temperature of the system decreases the time required for the NPs to exit the HNT significantly. This indicates that for high or low temperature applications, release profiles will be significantly different than at room temperature. Simulation studies show that a pH-dependence exists and that pH of the surrounding media can be used as a control parameter to vary the rate of diffusion of molecular species from multi-walled nanotubes.

The model was then used to simulate the diffusion/release profiles of NPs from rigid, defect-free HNTs with endcaps. Simulation results show a marked delay in the diffusion of dexamethasone from HNTs when the end stoppers are introduced when compared to normal release profiles and instantaneous powder dissolution. Simulation studies also show that release can be controlled or tuned by adding end caps with different types of pores with varying properties such as pore type (spherical with single opening, flat with single opening and flat perforated), pore sizes and charge. Simulations show the release of dexamethasone from 15 nm tubes takes about 25 hours for 90% of the content to be released. The addition of 3 nm and 5 nm pores delays the release to several days to months. Increase in pore radius leads to a progressive evolution towards diffusion from uncapped CNTs as expected. When the caps and the NPs are oppositely charged, the delay in release is even more significant. Similar results can also be observed when perforated pores are used.

This work lays out the ground for further studies in fields such as drug delivery and self-healing composites. This study is expected to lead to a recipe where the diffusion rate can be then controlled as needed. The effects of external parameters like pH on the release profiles were also studied.

CHAPTER 7

FUTURE WORK

One possible disadvantage of using HNTs for sustained release is that the lumen volume is about 10% of the total volume. This limits the loading efficiency of the HNTs. One possible work is using a sulfate acid etching of the halloysite lumen to increase the lumen diameter. However, while increasing the diameter does allow for loading greater quantities into the lumen, it also leads to the faster release of the loaded substance. It would be highly advantageous if this model could be modified and used to study the loading of NPs into the halloysites from different media and compare them to the release of the same particles in the same or different media to assess the loading and containment of the loaded NPs.

In this work, water is used as the media. A much-needed future work is the study of the release of NPs in different media and into solids. It is possible that when the HNTs are loaded and dried, under the right conditions, the NPs inside the HNTs coagulate and crystallize. This model can be extended to study the occurrence of this in HNTs. If present, this phase transition after loading would significantly impact the release profiles and is an area of interest for experimentalists working in the field.

This work concentrates on the diffusion of NPs from HNTs. Other nanotube like CNTs as well as liposomes, etc. can also be used. Another possible improvement to model can be made by incorporating porous tube walls for the NTs. HNTs have porous

walls and to be able to study the diffusion of NPs through the walls, the model needs to be modified significantly. In this model, the experimentally observed burst phase is accounted for by increasing the density of the NPs near the tube's openings. A detailed study of the geometry of the tube's opening and the mechanisms of NP released from tube's openings will lead to a better understanding of the exact nature of the burst phase.

Besides the possible extensions of this model to other applications of NP release from NTs, the algorithm that was developed can be slightly modified to apply to seemingly unrelated processes. One of the possible applications is the prediction of diffusion of NPs through hydrogels as they swell or collapse. The entire mechanism of particle diffusion can be applied as it follows the MC formalism developed in this dissertation. The modification that needs to be implemented in order to study hydrogels is in the geometry of material where the NPs are diffusing.

Another application is the prediction of diffusion of NPs through concrete pores under the influence of an externally applied electric or magnetic field. The NP binders are driven into the concrete pores to fill them up, and thereby not only making the concrete stronger, but also filling up the pores and stopping the influx of dangerous rust causing ions through the pores. This, in turn, protects the rebar and keeps the concrete structure strong for longer periods of time. The necessary computational model is almost identical to the one developed here, except that the interaction of the NP with an external field is necessary and that can be added with minor problems. Also, diffusion from outside of a cylindrical cavity as opposed to from the inside is necessary.

APPENDIX A

FLOW CHART OF THE ALGORITHM

FLOW CHART OF THE ALGORITHM

Figure 1 shows the flow chart of the algorithm used in our code for the model.

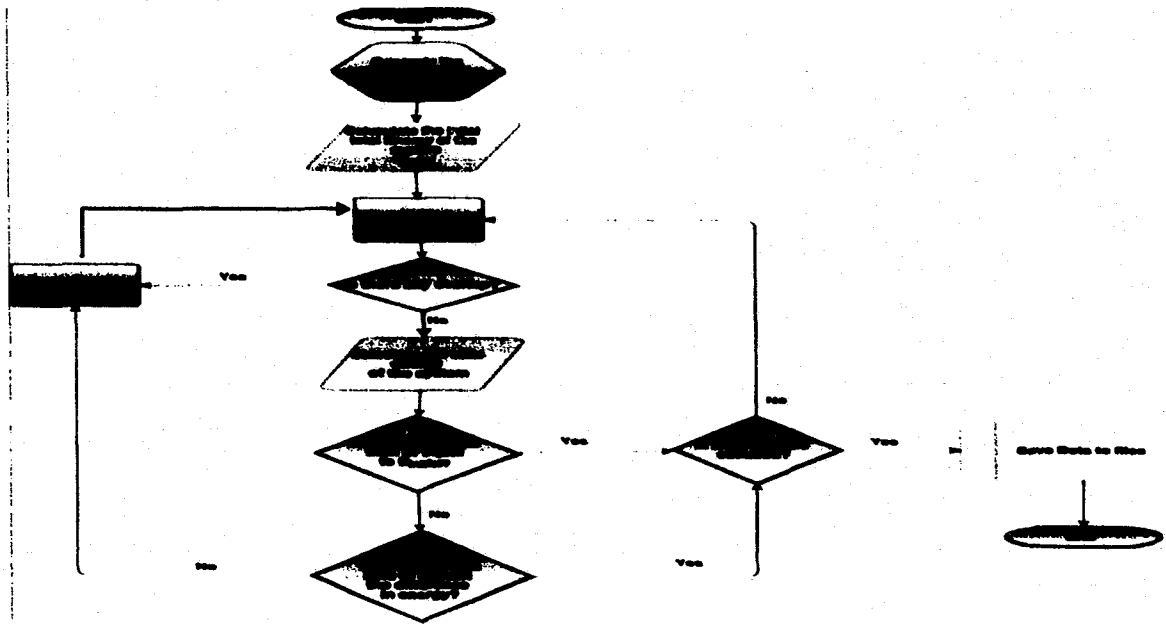


Figure A.1: Flow chart of the algorithm used in the model.

BIBLIOGRAPHY

- [1] Y. Yeo, *et al.*, "Microencapsulation methods for delivery of protein drugs," *Biotechnology and Bioprocess Engineering*, pp. 213-230, 2001.
- [2] G. Manish and S. Vimukta, "Targeted drug delivery system: A Review," *Res. Journal of Chemical Sciences*, vol. 1, 2011.
- [3] R. J. Chen, *et al.*, "Noncovalent sidewall functionalization of single-walled carbon nanotubes for protein immobilization," 20010717 DCOM- 20010809.
- [4] N. W. S. Kam and T. C. Jessop, "Nanotube molecular transporters: internalization of carbon nanotube-protein conjugates into mammalian cells," *Journal of the American Sciences*, pp. 6850-6851, 2004.
- [5] M. D. Brown, *et al.*, "Gene delivery with synthetic (non viral) carriers," 20011017 DCOM- 20011231.
- [6] M. E. Davis, "Non-viral gene delivery systems," *Current Opinion in Biotechnology*, vol. 13, pp. 128-131, 2002.
- [7] P. Jeyamohan, *et al.*, "Accelerated killing of cancer cells using a multifunctional single-walled carbon nanotube-based system for targeted drug delivery in combination with photothermal therapy," *International journal of nanomedicine*, vol. 8, pp. 2653-67, 2013.
- [8] J. V. Natarajan, *et al.*, "Sustained Drug Release in Nanomedicine: A Long-Acting Nanocarrier-Based Formulation for Glaucoma," *ACS nano*, 2014.
- [9] E. Abdullayev and Y. Lvov, "Halloysite clay nanotubes for controlled release of protective agents," *Journal of Nanosciences: Nanotechnol*, vol. 11, pp. 10007-26, Nov 2011.
- [10] Y. Huang, *et al.*, "Self-assembled particles of N-phthaloylchitosan-g-polycaprolactone molecular bottle brushes as carriers for controlled release of indometacin," *Journal of materials science. Materials in medicine*, vol. 21, pp. 557-65, 2010.
- [11] R. E. Whitmire, *et al.*, "Self-assembling nanoparticles for intra-articular delivery of anti-inflammatory proteins," *Biomaterials*, vol. 33, pp. 7665-75, 2012.

- [12] W. Aughenbaugh, *et al.*, "Silica sol-gel for the controlled release of antibiotics. II. The effect of synthesis parameters on the in vitro release kinetics of vancomycin," *Journal of Biomedical Materials Research*, vol. 57, pp. 321-326, 2001.
- [13] E. J. Anglin, *et al.*, "Porous silicon in drug delivery devices and materials," *Advances in Drug Delivery Review*, vol. 60, pp. 1266-1277, 2008.
- [14] C. Argyo, *et al.*, "Multifunctional Mesoporous Silica Nanoparticles as a Universal Platform for Drug Delivery," *Chemistry of Materials*, 2013.
- [15] S. A Mackowiak, *et al.*, "Targeted drug delivery in cancer cells with red-light photoactivated mesoporous silica nanoparticles," *Nano Letters*, vol. 13, pp. 2576-83, 2013.
- [16] R. P. Bagwe, *et al.*, "Improved drug delivery using microemulsions: rationale, recent progress, and new horizons," *Critical Reviews in therapeutic drug carrier systems*, vol. 18, pp. 77-140, 2001.
- [17] A. Patel, "Ocular drug delivery systems: An overview," *World Journal of Pharmacology*, vol. 2, pp. 47-47, 2013.
- [18] T. M. Allen and P. R. Cullis, "Liposomal drug delivery systems: From concept to clinical applications," *Advances in Drug Delivery Review*, vol. 65, pp. 36-48, 2013.
- [19] A. Lavasanifar, *et al.*, "Poly(ethylene oxide)-block-poly(L-amino acid) micelles for drug delivery," *Advances in Drug Delivery Review*, vol. 54, pp. 169-90, 2002.
- [20] W. Xu, *et al.*, "Polymeric micelles, a promising drug delivery system to enhance bioavailability of poorly water-soluble drugs," *Journal of Drug Delivery*, vol. 2013, pp. 340315-340315, 2013.
- [21] K. Mohan, *et al.*, "Ophthalmic microemulsion: A comprehensive review," *International Journal of Pharma and Bio Sciences*, vol. 3, pp. 1-13, 2012.
- [22] L. Ying, *et al.*, "Drug delivery to the ocular posterior segment using lipid emulsion via eye drop administration: effect of emulsion formulations and surface modification," *International Journal of Pharmaceuticals*, vol. 453, pp. 329-35, 2013.
- [23] S. H. Mostafavi and R. J. Babu, "Nano-Sized Drug Delivery," *Journal of Molecular Sciences*, 2013.
- [24] N. K. Sahu, *et al.*, "Biodegradable hydrogels in controlled drug delivery," *Polymer Science & Technology*, vol. 3, pp. 22-30, 2013.
- [25] H. H. Bae, *et al.*, "Bio-derived poly(γ -glutamic acid) nanogels as controlled anticancer drug delivery carriers," *J Microbiol Biotechnol*, vol. 22, pp. 1782-9, 2012.

- [26] J. Kost and R. Langer, "Responsive polymeric delivery systems," *Advances in Drug Delivery Review*, vol. 46, pp. 125-148, 2001.
- [27] J. W. Christopher, *et al.*, "Halloysite Nanoclay for Controlled Release Applications," in *Nanomaterials for Biomedicine*. vol. 1119, ed: American Chemical Society, 2012, pp. 209-238.
- [28] L. Lacerda, *et al.*, "Carbon nanotubes as nanomedicines: From toxicology to pharmacology," *Advances in Drug Delivery Review*, vol. 58, pp. 1460-1470, 2006.
- [29] M. Prato, *et al.*, "Functionalized Carbon Nanotubes in Drug Design and Discovery," *Accounts of Chemical Research*, vol. 41, pp. 60-68, 2007.
- [30] H. Dai, "Carbon nanotubes: synthesis, integration, and properties," *Accounts of Chemical Research*, vol. 35, pp. 1035-44, 2002.
- [31] R. Zhai, *et al.*, "Immobilization of enzyme biocatalyst on natural halloysite nanotubes," *Catalysis Communications*, vol. 12, pp. 259-263, 2010.
- [32] Y. Lvov, *et al.*, *ACS nano*, vol. 2, pp. 814, 2008.
- [33] D. Shchukin, *et al.*, *Small*, vol. 1, pp. 510, 2005.
- [34] S. R. Levis and P. B. Deasy, "Use of coated microtubular halloysite for the sustained release of diltiazem hydrochloride and propranolol hydrochloride," *International Journal of Pharmaceuticals*, vol. 253, pp. 145-57, 2003.
- [35] R. Price, *et al.*, *J. Microencapsulation*, vol. 18, pp. 713, 2001.
- [36] S. R. Levis and P. B. Deasy, "Characterisation of halloysite for use as a microtubular drug delivery system," *International Journal of Pharmaceuticals*, vol. 243, pp. 125-34, 2002.
- [37] H. M. Kelly, *et al.*, "Formulation and preliminary in vivo dog studies of a novel drug delivery system for the treatment of periodontitis," *International Journal of Pharmaceuticals*, vol. 274, pp. 167-83, 2004.
- [38] G. L. Li, *et al.*, "Silica/Polymer Double-Walled Hybrid Nanotubes: Synthesis and Application as Stimuli-Responsive Nanocontainers in Self-Healing Coatings," *ACS nano*, vol. 7, pp. 2470-2478, 2013.
- [39] E. Abdullayev and Y. Lvov, "Clay nanotubes for corrosion inhibitor encapsulation: release control with end stoppers," *Journal of Materials Chemistry*, vol. 20, pp. 6681-6687, 2010.

- [40] Y. Zhao, *et al.*, "Halloysite nanotubule clay for efficient water purification," *Journal of Colloid and Interface Science*, vol. 406, pp. 121-129, 2013.
- [41] G. Cavallaro, *et al.*, "Films of Halloysite Nanotubes Sandwiched between Two Layers of Biopolymer: From the Morphology to the Dielectric, Thermal, Transparency, and Wettability Properties," *The Journal of Physical Chemistry C*, vol. 115, pp. 20491-20498, 2011.
- [42] S. A. Hashemifard, *et al.*, "Mixed matrix membrane incorporated with large pore size halloysite nanotubes (HNT) as filler for gas separation: Experimental," *Journal of Colloid and Interface Science*, vol. 359, pp. 359-370, 2011.
- [43] E. Abdullayev, *et al.*, "Natural Tubule Clay Template Synthesis of Silver Nanorods for Antibacterial Composite Coating," *ACS Applied Material Interfaces*, vol. 3, pp. 4040-4046, 2011.
- [44] Y. Zhou, "Nanotubes: A New Carrier for Drug Delivery Systems," *The Open Nanoscience Journal*, vol. 2, pp. 1-5, 2008.
- [45] S. M. Garg and V. A. Deshmukh, "Carbon nanotubes—A novel drug delivery system," *International Journal of Research in Pharmacy and Chemistry*, vol. 2, pp. 523-532, 2012.
- [46] Y.-F. Shi, *et al.*, "Functionalized halloysite nanotube-based carrier for intracellular delivery of antisense oligonucleotides," *Nanoscale Research Letters*, vol. 6, pp. 608-608, 2011.
- [47] J. F. P. Leal, *et al.*, "Molecular Dynamics of Carbon Nanotube Bundles as Molecular Sieves," *Journal of Nanosciences Nanotechnology*, vol. 11, pp. 4934-4937, 2011.
- [48] F. Buyukserin and C. R. Martin, "The use of Reactive Ion Etching for obtaining "free" silica nano test tubes," *Applied Surface Science*, vol. 256, pp. 7700-7705, 2010.
- [49] A. Minett, *et al.*, "Nanotube actuators for nanomechanics," *Current Applied Physics*, vol. 2, pp. 61-64, 2002.
- [50] S. Jalili, *et al.*, "Ti-coated BC₂N nanotubes as hydrogen storage materials," *Canadian Journal of Chemistry*, vol. 91, pp. 598-604, 2013.
- [51] S. Santucci, *et al.*, "NO₂ and CO gas adsorption on carbon nanotubes: Experiment and theory," *The Journal of Chemical Physics*, vol. 119, pp. 10904, 2003.
- [52] P. He and L. Dai, "Carbon Nanotube Biosensors," in *BioMEMS and Biomedical Nanotechnology*, M. Ferrari, *et al.*, Eds., ed: Springer US, pp. 171-201, 2006.

- [53] T. W. Prow, *et al.*, "Nanoparticles, molecular biosensors, and multispectral confocal microscopy," *Journal of Molecular Histology*, vol. 35, pp. 555-64, 2004.
- [54] J. Montenegro, *et al.*, "Ion Channel Models Based on Self-Assembling Cyclic Peptide Nanotubes," *ACS Chemical Research*, vol. 30, pp. 30, 2013.
- [55] K. H. Park, "Single-walled Carbon Nanotubes Are a New Class of Ion Channel Blockers," *Journal of Biological Chemistry*, vol. 278, pp. 50212-50216, 2003.
- [56] Y. Jiao and P. Yang, "Molecular modeling of the ion channel-like nanotube structure of amyloid β -peptide," *Chinese Science Bulletin*, vol. 52, pp. 1576-1580, 2007.
- [57] T. G. Burke, *et al.*, "Entrapment of 6-Carboxyfluorescein within Cylindrical Phospholipid Microstructures," *Annals of the New York Academy of Sciences*, vol. 507, pp. 330-333, 1987.
- [58] R. Price and M. Patchan, "Controlled release from cylindrical microstructures," *Journal of Microencapsulation*, vol. 8, pp. 301-6, 1991.
- [59] b"Coating and composition containing lipid microstructure toxin dispensers," USA Patent, 1991.
- [60] J. Forsgren, *et al.*, "A ceramic drug delivery vehicle for oral administration of highly potent opioids," *Journal of Pharmaceutical Sciences*, vol. 99, pp. 219-226, 2010.
- [61] K. Malek and M.-O. Coppens, "Knudsen self- and Fickian diffusion in rough nanoporous media," *The Journal of Chemical Physics*, vol. 119, pp. 2801-2801, 2003.
- [62] K. Malek and M.-O. Coppens, "Knudsen self- and Fickian diffusion in rough nanoporous media," *The Journal of Chemical Physics*, vol. 119, pp. 2801-2811, 2003.
- [63] B. Hosticka, *et al.*, "Gas flow through aerogels," *Journal of Non-Crystalline Solids*, vol. 225, pp. 293-297, 1998.
- [64] D. N. Jaguste and S. K. Bhatia, "Combined surface and viscous flow of condensable vapor in porous media," *Chemical Engineering Science*, vol. 50, pp. 167-182, 1995.
- [65] M. Weber and R. Kimmich, "Maps of electric current density and hydrodynamic flow in porous media: NMR experiments and numerical simulations," *Physical Review E*, vol. 66, pp. 026306-026318, 2002.
- [66] F. Bao, *et al.*, "Simulation of gas flows in micro/nano systems using the Burnett equations," *Journal of Physics: Conference Series*, vol. 362, pp. 012031-012031, 2012.
- [67] A. Z. Akcasu, *et al.*, "Theory of Self Diffusion in Classical Fluids: The Van Hove Self Correlation Function $G(r, t)$," *Physics of Fluids*, 1970.

- [68] S. Roy, *et al.*, "Modeling gas flow through microchannels and nanopores," *Journal of Applied Physics*, vol. 93, pp. 4870-4879, 2003.
- [69] G. A. Bird, *Molecular Gas Dynamics and the Direct Simulation of Gas Flows*. Oxford, United Kingdom: Clarendon Press, 1994.
- [70] D. Jie, *et al.*, "Navier-Stokes simulations of gas flow in micro devices," *Journal of Micromechanics and Microengineering*, vol. 10, pp. 372-379, 2000.
- [71] S. A. Schaaf and P. L. Chambre, *Flow of rarefied gases*. Princeton, New Jersey: Princeton University Press, 1961.
- [72] H. Xue, *et al.*, "Prediction of Microchannel Flow Using Direct Simulation Monte Carlo," *Probabilistic Engineering Mechanics*, vol. 15, pp. 213-219, 2000.
- [73] J. C. Maxwell, "On stresses in rarefied gases arising from inequalities of temperature," *Philosophical Transactions of the Royal Society Part 1*, vol. 170, pp. 231-256, 1879.
- [74] Z. Mao and S. B. Sinnott, "A Computational Study of Molecular Diffusion and Dynamic Flow through Carbon Nanotubes," *The Journal of Physical Chemistry B*, vol. 104, pp. 4618-4624, 2000.
- [75] J. Koplik and J. R. Banavar, "Continuum Deductions from Molecular Hydrodynamics," *Annual Review of Fluid Mechanics*, vol. 27, pp. 257-292, 1995.
- [76] G. Karniadakis and A. Beskok, *Micro Flows-Fundamentals and Simulation*. New York: Springer-Verlag, 2002.
- [77] M. Gad-el-hak, "The Fluid Mechanics of Microdevices --- The Freeman Scholar Lecture," *Journal of Fluids Engineering*, vol. 121, pp. 5-33, 1999.
- [78] C. M. Ho and Y. C. Tai, "Micro-electro-mechanical systems (MEMS) and fluid flows," *Annual Review Fluid Mechanics*, vol. 30, pp. 579-612, 1998.
- [79] M. Friák, *et al.*, "Methodological challenges in combining quantum-mechanical and continuum approaches for materials science applications," *The European Physical Journal Plus*, vol. 126, pp. 101-101, 2011.
- [80] H.-S. Tsien, *Collected works of H. S. Tsien : 1938-1956*. Oxford: Academic Press, 2012.
- [81] E. S. Oran, *et al.*, "Direct Simulation Montecarlo: Recent Advances and Applications1," *Annual Review of Fluid Mechanics*, vol. 30, pp. 403-441, 1998.

- [82] R. K. Agarwal, *et al.*, "Beyond Navier–Stokes: Burnett equations for flows in the continuum–transition regime," *Physics of Fluids*, vol. 13, pp. 3061-3085, 2001.
- [83] E. J. Rosenbom, "The Mathematical Theory of Non-Uniform Gases (Chapman, S.; Cowling, T. G.)," *Journal of Chemical Education*, vol. 18, pp. 48-54, 1941.
- [84] C. K. Oh, *et al.*, "Computations of High-Speed, High Knudsen Number Microchannel Flows," *Journal of Thermophysics and Heat Transfer*, vol. 11, pp. 497-505, 1997.
- [85] B. J. Alder and T. E. Wainwright, "Phase Transition for a Hard Sphere System," *The Journal of Chemical Physics*, vol. 27, pp. 1208-1209, 1957.
- [86] M. Robert and C. Dean, "Stabilization of the Burnett equations and application to high-altitude hypersonic flows," in *29th Aerospace Sciences Meeting*, ed: American Institute of Aeronautics and Astronautics, 1991.
- [87] B. Fubing, *et al.*, "Simulation of gas flows in micro/nano systems using the Burnett equations," *Journal of Physics: Conference Series*, vol. 362, pp. 012031-012043, 2012.
- [88] T. Düren, *et al.*, "Composition dependent transport diffusion coefficients of CH₄/CF₄ mixtures ion carbon nanotube by nonequilibrium molecular dynamics simulations," *Chemical Engineering Science*, vol. 57, pp. 1343-1354, 2002.
- [89] D. S. Sholl and K. A. Fichthorn, "Normal, single-file, and dual-mode diffusion of binary adsorbate mixtures in AlPO₄-5," *The Journal of Chemical Physics*, vol. 107, pp. 4384-4389, 1997.
- [90] D. Keffer, "The temperature dependence of single-file separation mechanisms in one-dimensional nanoporous materials," *Chemical Engineering Journal*, vol. 74, pp. 33-42, 1999.
- [91] D. Nicholson, "A simulation study of the pore size dependence of transport selectivity in cylindrical pores," *Molecular Physics*, vol. 100, pp. 2151-2163, 2002.
- [92] R. E. Tuzun, *et al.*, "Dynamics of fluid flow inside carbon nanotubes," *Nanotechnology*, vol. 7, pp. 241-246, 1996.
- [93] Y. G. Seo, *et al.*, "Monte Carlo simulation of transport diffusion in nanoporous carbon membranes," *Journal of Membrane Science*, vol. 195, pp. 65-73, 2002.
- [94] A. ten Bosch, "Persistent diffusion in nanopores," *The Journal of Chemical Physics*, vol. 114, pp. 4982-4988, 2001.
- [95] D. M. C. Macewan, "Halloysite-organic Complexes," *Nature*, vol. 157 pp. 159-160, 1946.

- [96] Y. J. Suh, *et al.*, "Natural nanocontainer for the controlled delivery of glycerol as a moisturizing agent," *Journal of Nanosciences Nanotechnology*, vol. 11, pp. 661-665, 2011.
- [97] W. Liu, *et al.*, "Influence of the Length of Imogolite-Like Nanotubes on Their Cytotoxicity and Genotoxicity toward Human Dermal Cells," *Chemical Research in Toxicology*, vol. 25, pp. 2513-2522, 2012.
- [98] J. S. Rasul, "Chip on paper technology utilizing anisotropically conductive adhesive for smart label applications," *Microelectronics Reliability*, vol. 44, pp. 135-140, 2004.
- [99] E. Joussein, *et al.*, *Clay Minerals*, vol. 40, pp. 383-391, 2005.
- [100] G. Tari, *et al.*, *Journal of Colloid Interface Sciences*, vol. 210, pp. 360-369, 1999.
- [101] V. Vergaro, *et al.*, "Cytocompatibility and Uptake of Halloysite Clay Nanotubes," *Biomacromolecules*, vol. 11, pp. 820-826, 2010.
- [102] E. Abdullayev, *et al.*, *ACS Applied Material Interfaces*, vol. 2, pp. 1437-1443, 2009.
- [103] R. Kamble, *et al.*, "Halloysite Nanotubes and Applications: A Review," *Journal of Advanced Scientific Research*, vol. 3, pp. 435-445, 2012.
- [104] Y. Yang, *et al.*, *Biomaterials*, vol. 18, pp. 3083-3091, 2007.
- [105] N. Veerabadran, *et al.*, *NANO*, vol. 2, pp. 215-229, 2007.
- [106] N. Veerabadran, *et al.*, *Macromolecules Rapid Communications*, vol. 30, pp. 94-101, 2009.
- [107] Y. Lvov, *et al.*, *Langmuir*, vol. 12, pp. 3038-3042, 1996.
- [108] P. Liu and M. Zhao, *Applied Surface Sciences*, vol. 255, pp. 3989-3995, 2009.
- [109] M. Liu, *et al.*, *Nanotechnology*, vol. 19, pp. 205709-205718, 2008.
- [110] D. Kommireddy, *et al.*, *J. Biomed. Nanotechnol.*, vol. 1, pp. 286-294, 2005.
- [111] R. R. Price, *et al.*, "Controlled release from halloysite: a cylindrical mineral.," In *11th International Symposia on Microencapsulation*, Bangkok, Thailand, 1998.
- [112] H. M. Kelly, *et al.*, "Formulation and preliminary in vivo dog studies of a novel drug delivery system for the treatment of periodontitis," *International journal of pharmaceutics*, vol. 274, pp. 167-183, 2004.

- [113] N. G. Veerabadran, *et al.*, "Clay Nanotubes for Encapsulation and Sustained Release of Drugs," *NANO*, vol. 02, pp. 115-128, 2007.
- [114] V. Vergaro, *et al.*, "Drug-loaded polyelectrolyte microcapsules for sustained targeting of cancer cells," *Advances in Drug Delivery Reviews*, vol. 63, pp. 847-64, 2011.
- [115] K. Ariga, *et al.*, "Layer-by-layer self-assembled shells for drug delivery," *Advances in Drug Delivery Review*, vol. 63, pp. 762-71, 2011.
- [116] E. Abdullayev, *et al.*, "Natural tubule clay template synthesis of silver nanorods for antibacterial composite coating," *ACS Appl Mater Interfaces*, vol. 3, pp. 4040-6, 2011.
- [117] Y. M. Lvov, *et al.*, "Halloysite clay nanotubes for controlled release of protective agents," *ACS nano*, vol. 2, pp. 814-20, 2008.
- [118] S. Giri, *et al.*, "Stimuli-Responsive Controlled-Release Delivery System Based on Mesoporous Silica Nanorods Capped with Magnetic Nanoparticles," *Angewandte Chemie International Edition*, vol. 44, pp. 5038-5044, 2005.
- [119] G. Cavallaro, *et al.*, "Halloysite nanotube with fluorinated lumen: Non-foaming nanocontainer for storage and controlled release of oxygen in aqueous media," *Journal of Colloid and Interface Science*, vol. 417, pp. 66-71, 2014.
- [120] V. R. Cirkva, *et al.*, "Novel perfluoroalkylated derivatives of d-galactopyranose and xylitol for biomedical uses. Hemocompatibility and effect on perfluorocarbon emulsions," *Carbohydrate Research*, vol. 339, pp. 2177-2185, 2004.
- [121] E. Abdullayev, *et al.*, "Enlargement of halloysite clay nanotube lumen by selective etching of aluminum oxide," *ACS nano*, vol. 6, pp. 7216-26, 2012.
- [122] D. Borgis and R. Vuilleumier, "Transport and infrared spectroscopy of the hydrated proton.," *Abstracts of Papers of the American Chemical Society*, vol. 220, pp. U191-U191, 2000.
- [123] A. Afanasiev and V. Minogin, "van der Waals interaction of an atom with the internal surface of a hollow submicrometer-size cylinder," *Physical Review A*, vol. 82, 2010.
- [124] G. J. Tjatjopoulos, *et al.*, "Molecule-micropore interaction potentials," *The Journal of Physical Chemistry*, vol. 92, pp. 4006-4007, 1988.
- [125] N. S. Pujar and A. L. Zydney, "Charge Regulation and Electrostatic Interactions for a Spherical Particle in a Cylindrical Pore," *Journal of Colloidal Interface Sciences*, vol. 192, pp. 338-49, 1997.

- [126] W. Richard Bowen, *et al.*, "A model of the interaction between a charged particle and a pore in a charged membrane surface," *Advances in Colloid and Interface Science*, vol. 81, pp. 35-72, 1999.
- [127] J. E. Jones, "On the Determination of Molecular Fields. II. From the Equation of State of a Gas," *Proceedings of the Royal Society A: Mathematical, Physical and Engineering Sciences*, vol. 106, pp. 463-477, 1924.
- [128] L. Zhang and P. Winkler, "Debye-Hückel screening and fluctuations," *Chemical Physics*, vol. 329, pp. 338-342, 2006.
- [129] W. B. RUSSEL, *et al.*, "Colloidal Dispersions". *Journal of Fluid Mechanics*, vol. 222, pp. 692-694, 1989.
- [130] S. Chapman and T. G. Cowling, *The Mathematical Theory of Non-uniform Gases*: Cambridge 1991.
- [131] R. W. Korsmeyer, *et al.*, "Mechanisms of solute release from porous hydrophilic polymers," *International journal of pharmaceutics*, vol. 15, pp. 25-35, 1983.
- [132] T. Phaechamud, *et al.*, "Chitosan citrate as film former: compatibility with water-soluble anionic dyes and drug dissolution from coated tablet," *International journal of pharmaceutics*, vol. 198, pp. 97-111, 2000.
- [133] A. Waugh and A. Grant, Eds., *Anatomy and Physiology in Health and Illness*. Churchill Livingstone Elsevier, 2007.
- [134] W. Wenbo, "Halloysite nanotube composites for sustained release of antimicrobial agents (antiseptics and antibiotics)," Doctoral Dissertation 2013.
- [135] S. Bordeepong, *et al.*, "Characterization of halloysite from Thung Yai District, Nakhon Si Thammarat Province, in Southern Thailand," *Songklanakar in Journal of Science & Technology*, vol. 33, pp. 599-607, 2011.
- [136] S. H. Patterson and H. H. Murray, *Kaolin, refractory clay, ball clay, and halloysite in North America, Hawaii, and the Caribbean region / by Sam H. Patterson and Haydn H. Murray*: [Reston, Va.] : U.S. Dept. of the Interior, Geological Survey ; Alexandria, VA, USGS, 1984.
- [137] B. K. G. Theng, *et al.*, "Surface properties of allophane, halloysite, imogolite," *Clays and Clay Minerals*, vol. 30, pp. 143-149, 1982.
- [138] S. Kaufhold, *et al.*, "A new massive deposit of allophane raw material in Ecuador," *Clays and Clay Minerals*, vol. 57, pp. 72-81, 2009.

- [139] R. Nagarajan, Ed., *Nanomaterials for Biomedicine* (ACS Symposium Series 1119). American Chemical Society, 2012.
- [140] A. Joshi, *et al.*, "Optimization of Geopolymer Properties by Coating of Fly-Ash Microparticles with Nanoclays," *Journal of Inorganic and Organometallic Polymers and Materials*, pp. 1-11, 2014.
- [141] Qiu, Y., Park, K., "Environment-sensitive hydrogels for drug delivery," *Advances in Drug Delivery Reviews*, vol. 53, pp. 321-339, 2001.
- [142] Soppimath, *et al.*, "Stimulus-responsive smart hydrogels as novel drug delivery systems," *Drug Developments in Industrial Pharmaceuticals*, vol. 28, pp. 957-974 2002.
- [143] Chilkoti, A., *et al.*, "Targeted drug delivery by thermally responsive polymers," *Advances in Drug Delivery Reviews*, vol. 54, pp. 613-630, 2002.
- [144] Thornton, P.D., *et al.*, "Enzyme-responsive polymer hydrogel particles for controlled release," *Advanced Materials*, vol. 19, pp. 1252-1256, 2007.
- [145] Qu, T.H., *et al.*, "Preparation of an amphiphilic triblock copolymer with pH- and thermo-responsiveness and self-assembled micelles applied to drug release," *Journal of Colloid Interface Sciences*, vol. 336, pp. 865-871, 2009.
- [146] Zhang, N.Y., *et al.*, "Preparation, properties, and drug release of thermo- and pH-sensitive poly ((2-dimethylamino) ethyl methacrylate)/poly (N,N-diethyl acrylamide) semi-IPN hydrogels," *Journal of Material Sciences*, vol. 46, pp.1523-1534, 2011.
- [147] Zhang, X.G., *et al.*, "Glucosamine-carrying temperature- and pH-sensitive microgels: Preparation, characterization, and in vitro drug release studies," *Journal of Colloid Interface Sciences*, vol. 322, pp.333-341, 2008.
- [148] D. Grahame, "The electrical double layer and the theory of electro-capillarity," *Chemical Reviews*, pp: 441-445, 1947.